J|A|C|S ARTICLES

Published on Web 03/01/2010

Redox-Active Ligands Facilitate Bimetallic O_2 Homolysis at Five-Coordinate Oxorhenium(V) Centers

Cameron A. Lippert,[†] Stephen A. Arnstein,[†,‡,§] C. David Sherrill,*[,†,‡,§] and Jake D. Soper*[,†]

School of Chemistry and Biochemistry, Center for Computational Molecular Science and Technology, and College of Computing, Georgia Institute of Technology, Atlanta, Georgia 30332-0400

Received December 12, 2009; E-mail: jake.soper@chemistry.gatech.edu; sherrill@gatech.edu

Abstract: Five-coordinate oxorhenium(V) anions with redox-active catecholate and amidophenolate ligands are shown to effect clean bimetallic cleavage of O_2 to give dioxorhenium(VII) products. A structural homologue with redox-inert oxalate ligands does not react with O_2. Redox-active ligands lower the kinetic barrier to bimetallic O_2 homolysis at five-coordinate oxorhenium(V) by facilitating formation and stabilization of intermediate O_2 adducts. O_2 activation occurs by two sequential Re−O bond forming reactions, which generate mononuclear η^1-superoxo species, and then binuclear *trans*-μ-1,2-peroxo-bridged complexes. Formation of both Re−O bonds requires trapping of a triplet radical dioxygen species by a *cis*-$[Re^V(O)(cat)_2]^-$ anion. In each reaction the dioxygen fragment is reduced by $1e^-$, so generation of each new Re−O bond requires that an oxometal fragment is oxidized by $1e^-$. Complexes containing a redox-active ligand access a lower energy reaction pathway for the $1e^-$ Re−O bond forming reaction because the metal fragment can be oxidized without a change in formal rhenium oxidation state. It is also likely that redox-active ligands facilitate O_2 homolysis by lowering the barrier to the formally spin-forbidden reactions of triplet dioxygen with the closed shell oxorhenium(V) anions. By orthogonalizing $1e^-$ and $2e^-$ redox at oxorhenium(V), the redox-active ligand allows high-valent rhenium to utilize a mechanism for O_2 activation that is atypical of oxorhenium(V) but more typical for oxygenase enzymes and models based on 3d transition metal ions: O_2 cleavage occurs by a net $2e^-$ process through a series of $1e^-$ steps. The implications for design of new multielectron catalysts for oxygenase-type O_2 activation, as well as the microscopic reverse reaction, O−O bond formation from coupling of two M═O fragments for catalytic water oxidation, are discussed.

Introduction

Selective oxidation reactions are utilized for transformations of small molecules in applications ranging from benchtop-scale laboratory synthesis, to pharmaceuticals production, to the manufacture of petroleum products.[1−8] Molecular oxygen is the ideal inexpensive and environmentally benign oxidant, and there are now many examples of selective and powerful transition metal catalysts for aerobic partial oxidations of organic substrates.[9−24] Although many of these synthetic systems are

[†] School of Chemistry and Biochemistry.
[‡] Center for Computational Molecular Science and Technology.
[§] College of Computing.

(1) Sheldon, R. A.; Kochi, J. K. *Metal-Catalyzed Oxidations of Organic Compounds*; Academic Press: New York, 1981.
(2) *Comprehensive Organic Synthesis: Selectivity, Strategy and Efficiency in Modern Organic Chemistry Volume 7: Oxidation*; Trost, B. M., Fleming, I., Eds.; Pergamon: Oxford, U.K., 1991.
(3) *Organic Syntheses by Oxidation with Metal Compounds*; Mijs, W. J., De Jonge, C. R. H. I., Eds.; Plenum: New York, 1986.
(4) Cavani, F.; Ballarini, N.; Luciani, S. *Top. Catal.* **2009**, *52*, 935–947.
(5) Parshall, G. W.; Ittel, S. D. Homogeneous Catalysis. *The Applications and Chemistry of Catalysis by Soluble Transition Metal Complexes*, 2nd ed.; Wiley-Interscience: New York, 1992.
(6) Haber, J. In *Handbook of Heterogenous Catalysis*, 2nd ed.; Ertl, G., Ed.; Wiley-VCH: Weinheim, Germany, 2008; Vol. 7, pp 3359−3384.
(7) Van Deurzen, M. P. J.; Van Rantwijk, F.; Sheldon, R. A. *Tetrahedron* **1997**, *53*, 13183–13220.
(8) Whittall, J. In *Catalysts for Fine Chemical Synthesis*; Roberts, S. M., Whittall, J., Eds.; John Wiley & Sons Ltd.: Chichester, U.K., 2007; Vol. 5, pp 1−33.
(9) *Oxygen Complexes and Oxygen Activation by Transition Metals*; Martell, A. E., Sawyer, D. T., Eds.; Plenum: New York, 1988.
(10) *The Activation of Dioxygen and Homogeneous Catalytic Oxidation*; Barton, D., H. R., Martell, A. E., Sawyer, D. T., Eds.; Plenum: New York, 1993.
(11) Boring, E.; Geletii, Y. V.; Hill, C. L. *Catal. Met. Complexes* **2003**, *26*, 227–264.
(12) Dijksman, A.; Arends, I. W. C. E.; Sheldon, R. A. *Platinum Met. Rev.* **2001**, *45*, 15–19.
(13) Murahashi, S.-I.; Komiya, N.; Hayashi, Y.; Kumano, T. *Pure Appl. Chem.* **2001**, *73*, 311–314.
(14) Zhan, B.-Z.; Thompson, A. *Tetrahedron* **2004**, *60*, 2917–2935.
(15) Stahl, S. S. *Angew. Chem., Int. Ed.* **2004**, *43*, 3400–3420.
(16) Stahl, S. S. *Science* **2005**, *309*, 1824–1826.
(17) *Advances in Catalytic Activation of Dioxygen by Metal Complexes*; Simandi, L. I., Ed.; Kluwer Acadmic Publishers: Norwell, MA, 2003.
(18) Borovik, A. S.; Zinn, P. J.; Zart, M. K. In *Activation of Small Molecules: Organometallic and Bioinorganic Perspectives*; Tolman, W. B., Ed.; Wiley-VCH: Weinheim, Germany, 2006; pp 187−234.
(19) Nam, W. *Acc. Chem. Res.* **2007**, *40*, 465.
(20) Chaudhuri, P.; Wieghardt, K.; Weyhermueller, T.; Paine, T. K.; Mukherjee, S.; Mukherjee, C. *Biol. Chem.* **2005**, *386*, 1023–1033.
(21) Chaudhuri, P.; Hess, M.; Mueller, J.; Hildenbrand, K.; Bill, E.; Weyhermueller, T.; Wieghardt, K. *J. Am. Chem. Soc.* **1999**, *121*, 9599–9610.
(22) Wang, Y.; DuBois, J. L.; Hedman, B.; Hodgson, K. O.; Stack, T. D. P. *Science* **1998**, *279*, 537–540.

Scheme 1

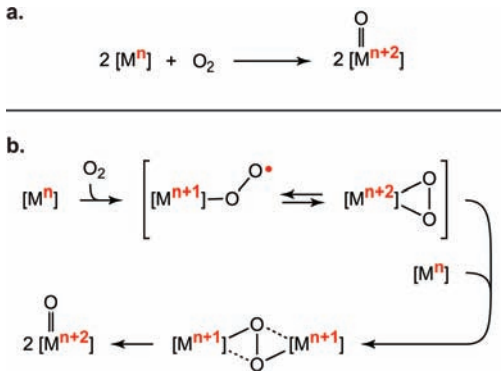

well understood, the chemical features that engender selective O_2 reduction are often not easily transferrable to other classes of oxidation catalysts. Therefore, the development of general methods for activation of O_2 presages systematic development of new catalytic cycles for aerobic oxidations of small organic molecules.

Biological systems that utilize O_2 as a terminal oxidant have received extensive attention for their ability to mediate a wide variety of selective oxidation reactions.[17,24–30] Accordingly, many recent efforts to effect enzyme-like selectivity in other aerobic oxidations take inspiration from biology by mimicking key structural and chemical properties that impart specificity in reactions with small molecule substrates.[10,17,22,24,25,30–35] A common step in oxygenase-type redox catalysis cycles is cleavage of the dioxygen O−O bond to generate a transition metal oxo complex.[18,19,24,25,27,36,37] Conversion of two metal ions and one O_2 molecule to two oxometal species is formally a $4e^-$ reduction of O_2 and a $2e^-$ oxidation of each metal fragment (Scheme 1a). Such bimetallic O_2 activation is frequently seen in both metalloenzymes and model systems containing naturally abundant transition metal ions.[18,19,25] Despite the diversity of active site structures, most studies of enzymatic and enzyme-like O_2 homolysis invoke a remarkably similar reaction mechanism. This "unified scheme"[19] proposes that O−O bond homolysis occurs by a series of sequential, metal-mediated $1e^-$ steps, via superoxo $[O_2^{\bullet}]^-$ and peroxo $[O_2]^{2-}$ complex intermediates. As illustrated in Scheme 1b for bimetallic O_2 homolysis, the intermediacy of both mononuclear superoxo complexes and symmetric dinuclear peroxo-bridged intermediates demands formal oxidation of each transition metal ion by $1e^-$. This reaction pattern reflects the fact most first row transition metal ions prefer to exist in oxidation states that vary by only $1e^-$,[38] so the preferred redox reaction for nearly all 3d transition metals is $1e^-$ transfer.

Metal-mediated oxygen-atom transfer is a $2e^-$ redox process,[39] so the utility of many coordinatively unsaturated 4d and 5d transition metal complexes in stoichiometric and catalytic oxo transfer reactions[1–5,40] derives in part from their ability to mediate the transfer of multiple electrons while avoiding odd-electron intermediates.[39,41–43] O_2 homolysis to generate a terminal metal oxo is formally abstraction of an oxygen-atom from dioxygen. Accordingly, the properties that facilitate oxo transfer processes at low-coordinate 4d and 5d metals also seem conducive to bimetallic O_2 cleavage: a strong thermodynamic proclivity for $2e^-$ redox changes and low d-electron counts that stabilize the resulting terminal oxo group.[39,44] Although reactions of second and third row transition metals to homolyze O_2 are not rare,[39,43,45–47] many thermodynamically strong oxygen-atom acceptors are stable in O_2.[39,48] We speculated that the propensity of some high-valent 4d and 5d metals to avoid odd-electron intermediates might introduce a kinetic barrier to symmetric bimetallic O_2 homolysis by inhibiting access to superoxo $[O_2^{\bullet}]^-$ and peroxo $[O_2]^{2-}$ complex intermediates. We proposed that coordination of a redox-active ligand to a high-valent 4d or 5d transition metal ion that is a strong $2e^-$ oxygen-atom acceptor may provide a route to overcome this barrier by giving access to the $1e^-$ steps for enzyme-like bimetallic O_2 activation.

The use of redox-active chelates as reservoirs of electrons in reactions at coordinatively unsaturated metals is an emerging strategy for selective redox transformations of small molecules, including O_2.[21,49–63] As shown in Scheme 2, these so-called

(23) Cornell, C. N.; Sigman, M. S. In *Activation of Small Molecules: Organometallic and Bioinorganic Perspectives*; Tolman William, B., Ed.; Wiley-VCH: Weinheim, Germany, 2006; pp 159−186.
(24) *Biomimetic Oxidations Catalyzed by Transition Metal Complexes*; Meunier, B., Ed.; Imperial College: London, 2000.
(25) Special Issue on Dioxygen Activation and Metallozyme Models, *Acc. Chem. Res.* **2007**, *40*, 465–634.
(26) Que, L., Jr.; Tolman, W. B. *Nature* **2008**, *455*, 333–340.
(27) *Porphyrin Handbook*; Kadish, K. M., Smith, K. M., Guilard, R., Eds.; Academic Press: San Diego, CA, 2000.
(28) Mirica, L. M.; Ottenwaelder, X.; Stack, T. D. P. *Chem. Rev.* **2004**, *104*, 1013–1045.
(29) Kopp, D. A.; Lippard, S. J. *Curr. Opin. Chem. Biol.* **2002**, *6*, 568–576.
(30) Tshuva, E. Y.; Lippard, S. J. *Chem. Rev* **2004**, *104*, 987–1012.
(31) Op't Holt, B. T.; Vance, M. A.; Mirica, L. M.; Heppner, D. E.; Stack, T. D. P.; Solomon, E. I. *J. Am. Chem. Soc.* **2009**, *131*, 6421–6438.
(32) Lewis, E. A.; Tolman, W. B. *Chem. Rev.* **2004**, *104*, 1047–1076.
(33) Kim, E.; Chufan, E. E.; Kamaraj, K.; Karlin, K. D. *Chem. Rev.* **2004**, *104*, 1077–1134.
(34) Costas, M.; Mehn Mark, P.; Jensen Michael, P.; Que, L., Jr. *Chem. Rev.* **2004**, *104*, 939–86.
(35) Sono, M.; Roach, M. P.; Coulter, E. D.; Dawson, J. H. *Chem. Rev.* **1996**, *96*, 2841–2887.
(36) Meunier, B.; de Visser, S. P.; Shaik, S. *Chem. Rev.* **2004**, *104*, 3947–3980.
(37) MacBeth, C. E.; Golombek, A. P.; Young, V. G., Jr.; Yang, C.; Kuczera, K.; Hendrich, M. P.; Borovik, A. S. *Science* **2000**, *289*, 938–941.
(38) Greenwood, N. N.; Earnshaw, A. *Chemistry of the Elements*; Pergamon: New York, 1984.
(39) Holm, R. H. *Chem. Rev.* **1987**, *87*, 1401–49.
(40) Kolb, H. C.; Sharpless, K. B. In *Transition Metals in Organic Synthesis*, 2nd ed.; Beller, M., Bolm, C., Eds.; Wiley-VCH: Weinheim, Germany, 2004; Vol. 2, p 275−298.
(41) Holm, R. H.; Donahue, J. P. *Polyhedron* **1993**, *12*, 571–89.
(42) Enemark, J. H.; Cooney, J. J. A.; Wang, J.-J.; Holm, R. H. *Chem. Rev.* **2004**, *104*, 1175–1200.
(43) Jacobi, B. G.; Laitar, D. S.; Pu, L.; Wargocki, M. F.; DiPasquale, A. G.; Fortner, K. C.; Schuck, S. M.; Brown, S. N. *Inorg. Chem.* **2002**, *41*, 4815–4823.
(44) Nugent, W. A.; Mayer, J. M. *Metal-Ligand Multiple Bonds*; John Wiley & Sons: New York, 1988.
(45) Harlan, E. W.; Berg, J. M.; Holm, R. H. *J. Am. Chem. Soc.* **1986**, *108*, 6992–7000.
(46) Neithamer, D. R.; LaPointe, R. E.; Wheeler, R. A.; Richeson, D. S.; Van Duyne, G. D.; Wolczanski, P. T. *J. Am. Chem. Soc.* **1989**, *111*, 9056–72.
(47) Brown, S. N.; Mayer, J. M. *Inorg. Chem.* **1992**, *31*, 4091–100.
(48) Espenson, J. H. *Adv. Inorg. Chem.* **2003**, *54*, 157–202.
(49) Blackmore, K. J.; Ziller, J. W.; Heyduk, A. F. *Inorg. Chem.* **2005**, *44*, 5559–61.
(50) Haneline, M. R.; Heyduk, A. F. *J. Am. Chem. Soc.* **2006**, *128*, 8410–1.
(51) Blackmore, K. J.; Lal, N.; Ziller, J. W.; Heyduk, A. F. *J. Am. Chem. Soc.* **2008**, *130*, 2728–9.
(52) Ketterer, N. A.; Fan, H.; Blackmore, K. J.; Yang, X.; Ziller, J. W.; Baik, M. H.; Heyduk, A. F. *J. Am. Chem. Soc.* **2008**, *130*, 4364–74.
(53) Zarkesh, R. A.; Ziller, J. W.; Heyduk, A. F. *Angew. Chem., Int. Ed. Engl.* **2008**, *47*, 4715–8.

Scheme 2

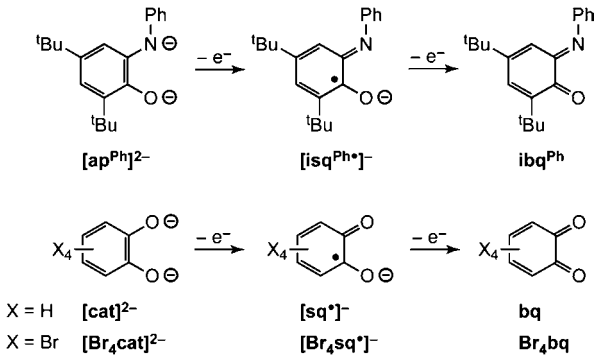

"non-innocent" ligands can coordinate as fully reduced catecholates $[cat]^{2-}$, partially oxidized semiquinonate free radicals $[sq^{\bullet}]^{-}$, and fully oxidized benzoquinones [bq].[64,65] When the energies of the redox-active ligand frontier orbitals are close to the metal ion frontier orbitals, low-energy intravalence charge transfer[65–69] can be utilized for stoichiometric and catalytic reactions at the metal center. In many ways this reactivity mirrors that widely seen in metalloporphyrins, especially O_2 reduction.[24,27,36] However, the redox-active chelates shown in Scheme 2 are easily prepared and offer the advantages of a high degree of flexibility in coordination environment and electronic tunability.

Five-coordinate oxorhenium(V) complexes have been extensively employed as oxo-transfer reagents,[39,48,70–72] but they generally do not react with dioxygen.[48] We were therefore intrigued by a report on the synthesis and characterization of oxorhenium complexes with redox-active catecholate ligands that noted the five-coordinate monooxo anion $[Re^{V}(O)(cat)_2]^{-}$ ($[cat]^{2-}$ = 1,2-catecholate; Scheme 2) is oxidized to the *cis*-dioxo complex $[Re^{VII}(O)_2(cat)_2]^{-}$ with exposure to air.[73] Reported herein are mechanistic and computational studies of O_2 cleavage by $[Re^{V}(O)(cat)_2]^{-}$ and related five-coordinate oxorhenium(V) complexes to yield dioxorhenium(VII) products. Data are presented that suggest bimetallic O_2 homolysis occurs through redox-active ligand-mediated $1e^{-}$ steps that mirror O−O bond cleavage by oxygenase enzymes. This ability of the redox-active ligands to deliver $1e^{-}$ imparts a remarkable radical-like reactivity to the closed-shell $[Re^{V}(O)(cat)_2]^{-}$ fragment, which in turn keys efficient Re−O bond formation via reactions with oxygen radicals. Moreover, the ability of the ligands to act as reservoirs for $1e^{-}$ does not perturb the ability of the oxorhenium(V) ion to effect $2e^{-}$ oxygen-atom transfer. This strategy to orthogonalize the $1e^{-}$ and $2e^{-}$ redox reactions for O_2 cleavage has implications for the design of new oxygenase catalysts. It is also important for the microscopic reverse reaction, coupling of oxometal fragments to evolve O_2, which is a key step in functional water oxidation catalysts and in natural and artificial photosynthetic systems.[74–84]

Experimental Details

General Considerations. Unless otherwise specified, all manipulations were performed under anaerobic conditions using standard vacuum line techniques or in an inert atmosphere glovebox under purified nitrogen. Routine NMR spectra were acquired on a Varian Mercury 300 spectrometer (300.323 MHz for ^{1}H; 75.5 MHz for ^{13}C) or a Varian Mercury 400 spectrometer (161.9 MHz for ^{31}P) at ambient temperature. Variable temperature NMR spectra were obtained with a Bruker AMX 400 spectrometer (400.138 MHz for ^{1}H). All chemical shifts are reported in parts per million (ppm) relative to TMS, with the residual solvent peak serving as an internal reference. UV−visible absorption spectra were acquired using a Varian Cary 50 spectrophotometer. Unless otherwise noted, all electronic absorption spectra were recorded at ambient temperatures in 1 cm quartz cells. UV−vis chemical kinetics data were fit by iterative multivariate analysis using the commercially available software Specfit/32 from Spectrum Software Associates. IR spectra were obtained in KBr or Nujol using a Shimadzu 8400S Fourier-transform infrared spectrophotometer or a Perkin-Elmer 1000 FT-IR spectrophotometer. All mass spectra were recorded in the Georgia Institute of Technology Bioanalytical Mass Spectrometry Facility. Electrospray ionization mass spectrometry (ESI-MS) was carried out with acetonitrile solutions using a Micromass Quattro LC spectrometer. Electron impact mass spectra (EI-MS) were obtained using a VG instruments model 70-SE spectrometer. Fast atom bombardment mass spectra (FAB-MS) were acquired in the negative mode on a VG Instruments 70-SE spectrometer. Elemental analyses were performed by Atlantic Microlab, Inc., Norcross, GA. All analyses were performed in duplicate, and the reported compositions are the average of the two runs.

(54) Nguyen, A. I.; Blackmore, K. J.; Carter, S. M.; Zarkesh, R. A.; Heyduk, A. F. *J. Am. Chem. Soc.* **2009**.
(55) Bart, S. C.; Lobkovsky, E.; Bill, E.; Chirik, P. J. *J. Am. Chem. Soc.* **2006**, *128*, 5302–5303.
(56) Bouwkamp, M. W.; Bowman, A. C.; Lobkovsky, E.; Chirik, P. J. *J. Am. Chem. Soc.* **2006**, *128*, 13340–13341.
(57) Bart, S. C.; Bowman, A. C.; Lobkovsky, E.; Chirik, P. J. *J. Am. Chem. Soc.* **2007**, *129*, 7212–7213.
(58) Stanciu, C.; Jones, M. E.; Fanwick, P. E.; Abu-Omar, M. M. *J. Am. Chem. Soc.* **2007**, *129*, 12400–1.
(59) Mukherjee, C.; Weyhermueller, T.; Bothe, E.; Chaudhuri, P. *Inorg. Chem.* **2008**, *47*, 2740–2746.
(60) Lu, C. C.; Weyhermueller, T.; Bill, E.; Wieghardt, K. *Inorg. Chem.* **2009**, *48*, 6055–6064.
(61) Chaudhuri, P.; Hess, M.; Weyhermueller, T.; Wieghardt, K. *Angew. Chem., Int. Ed.* **1999**, *38*, 1095–1098.
(62) Rolle, C. J.; Hardcastle, K. I.; Soper, J. D. *Inorg. Chem.* **2008**, *47*, 1892–1894.
(63) Smith, A. L.; Soper, J. D. *Polyhedron* **2010**, *29*, 164–169.
(64) Pierpont, C. G.; Lange, C. W. *Prog. Inorg. Chem.* **1994**, *41*, 331–442.
(65) Pierpont, C. G. *Coord. Chem. Rev.* **2001**, *216−217*, 99–125.
(66) Kokatam, S.-L.; Chaudhuri, P.; Weyhermueller, T.; Wieghardt, K. *Dalton Trans.* **2007**, 373–8.
(67) Ray, K.; Petrenko, T.; Wieghardt, K.; Neese, F. *Dalton Trans.* **2007**, 1552–1566.
(68) Hendrickson, D. N.; Pierpont, C. G. *Top. Curr. Chem.* **2004**, *234*, 63–95.
(69) Shultz, D. A. *Comments Inorg. Chem.* **2002**, *23*, 1–21.
(70) Owens, G. S.; Arias, J.; Abu-Omar, M. M. *Catal. Today* **2000**, *55*, 317–363.
(71) Arias, J.; Newlands, C. R.; Abu-Omar, M. M. *Inorg. Chem.* **2001**, *40*, 2185–2192.
(72) Herrmann, W. A.; Kuhn, F. E. *Acc. Chem. Res.* **1997**, *30*, 169–180.
(73) Dilworth, J. R.; Ibrahim, S. K.; Khan, S. R.; Hursthouse, M. B.; Karaulov, A. A. *Polyhedron* **1990**, *9*, 1323–9.
(74) Brudvig, G. W.; Beck, W. F.; De Paula, J. C. *Annu. Rev. Biophys. Biophys. Chem.* **1989**, *18*, 25–46.
(75) Eisenberg, R.; Gray, H. B. *Inorg. Chem.* **2008**, *47*, 1697–9.
(76) Surendranath, Y.; Dinca, M.; Nocera, D. G. *J. Am. Chem. Soc.* **2009**, *131*, 2615–2620.
(77) Betley, T. A.; Wu, Q.; Van Voorhis, T.; Nocera Daniel, G. *Inorg. Chem.* **2008**, *47*, 1849–61.
(78) *Comprehensive Series in Photochemical & Photobiological Sciences*; Renger, G., Ed.; Springer: New York, 2008.
(79) Tagore, R.; Crabtree, R. H.; Brudvig, G. W. *Inorg. Chem.* **2008**, *47*, 1815–1823.
(80) McEvoy, J. P.; Brudvig, G. W. *Chem. Rev.* **2006**, *106*, 4455–4483.
(81) Yagi, M.; Syouji, A.; Yamada, S.; Komi, M.; Yamazaki, H.; Tajima, S. *Photochem. Photobiol. Sci.* **2009**, *8*, 139–147.
(82) Ruettinger, W.; Dismukes, G. C. *Chem. Rev.* **1997**, *97*, 1–24.
(83) Liu, F.; Concepcion, J. J.; Jurss, J. W.; Cardolaccia, T.; Templeton, J. L.; Meyer, T. J. *Inorg. Chem.* **2008**, *47*, 1727–1752.
(84) Binstead, R. A.; Chronister, C. W.; Ni, J.; Hartshorn, C. M.; Meyer, T. J. *J. Am. Chem. Soc.* **2000**, *122*, 8464–8473.

Methods and Materials. Anhydrous acetonitrile (MeCN), dichloromethane, and pentane solvents for air- and moisture-sensitive manipulations were purchased from Sigma-Aldrich and further dried by passage through columns of activated alumina, degassed by at least three freeze−pump−thaw cycles, and stored under N_2 prior to use. Methanol (anhydrous, 99.0%) was purchased from Honeywell Burdick and Jackson. Ethanol (anhydrous, 200 proof, 99.5%) was purchased from Sigma-Aldrich. Acetone (99.8%, extra dry) was purchased from Acros. All were used as received. Oxygen (ultra high purity) was used as received from Airgas, Inc. Deuterated acetonitrile (MeCN-d_3) was purchased from Cambridge Isotope Laboratories, degassed by three freeze−pump−thaw cycles, vacuum distilled from CaH_2, and stored under a dry N_2 atmosphere prior to use. $Re^{V}(O)(PPh_3)_2Cl_3$,[85] $(Et_4N)[Re^{V}(O)(cat)_2]$,[86] $(Et_4N)[Re^{V}(O)(PPh_3)(cat)_2]$,[86] $(Et_4N)[Re^{VII}(O)_2(cat)_2]$,[73] $(^{n}Bu_4N)[Re^{V}(O)(OPPh_3)(Br_4cat)_2]$,[87] and 2,4-di-*tert*-butyl-6-(phenylamino)phenol (H_2ap^{Ph}; Scheme 2)[88] were prepared by literature methods. All characterization data matched those referenced. All other reagents were purchased from Sigma-Aldrich and used as received.

Preparation of $(Me_4N)[Re^{V}(O)(ap^{Ph})_2]$. A 50 mL flask with a Kontes brand high-vacuum PTFE valve was charged with $[Re^{V}O(PPh_3)_2Cl_3]$ (0.251 g, 0.302 mmol), Me_4NCl (0.242 g, 2.22 mmol), H_2ap^{Ph} (0.181 g, 0.608 mmol), and MeOH (10 mL). Et_3N (180 μL, 1.29 mmol) was slowly added with vigorous stirring to afford a green suspension. The flask was sealed and immersed in a silicone fluid bath at 85 °C for 4 h to yield a clear, dark green solution, then slowly cooled to ambient temperature, and stored under N_2 for 15 h to precipitate the desired product. Filtration through a fritted funnel afforded lime green crystals of $(Me_4N)[Re^{V}(O)(ap^{Ph})_2]$ (0.196 g, 0.226 mmol, 75%). UV−vis (MeCN) λ_{max}, nm (ε, M^{-1} cm^{-1}): 316 (19000), 620 (40). ^{1}H NMR (300 MHz, MeCN-d_3, δ): 7.34, 7.26 (br, N*Ph*: ortho, meta, 8H); 7.09 (t, J = 7 Hz, N*Ph*: para, 2H); 6.74 (d, J = 2 Hz, Ar*H*, 2H); 6.53 (d, J = 2 Hz, Ar*H*, 2H); 3.02 (s, Me_4N^+, 12H); 1.17 (s, −C(CH_3)$_3$, 9H); 1.02 (s, −C(CH_3)$_3$, 9H). Samples of $[Re^{V}(O)(ap^{Ph})_2]^-$ for elemental analysis contained 1 molecule of MeOH. MeOH is also observed in the X-ray crystal structure. The reported analysis is for $(Me_4N)[Re^{V}(O)(ap^{Ph})_2]\cdot$MeOH. Anal. Calcd for $C_{45}H_{66}N_3O_4Re$: C, 60.11; H, 7.40; N, 4.67; Found: C, 60.23; H, 7.35; N, 4.85.

Preparation of $(Et_3NH)[Re^{V}(O)(PPh_3)(ox)_2]$. $[Re^{V}(O)(PPh_3)_2Cl_3]$ (0.251 g, 0.300 mmol) and oxalic acid dihydrate ($H_2ox\cdot 2H_2O$) (0.075 g, 0.590 mmol) were combined in air with anhydrous EtOH (15 mL) in a 50 mL round-bottom flask, and Et_3N (165 μL, 1.18 mmol) was added dropwise with vigorous stirring. The resulting green suspension was heated to reflux to give a clear green solution that became violet over 40 min. The solution was cooled to room temperature and stored at 8 °C for 15 h to yield finely divided purple solids, which were collected by vacuum filtration. The solids were purified by precipitation from CH_2Cl_2 with pentane, affording microcrystalline $(Et_3NH)[Re^{V}(O)(PPh_3)(ox)_2]$ (0.169 g, 0.223 mmol, 87%). UV−vis (MeCN) λ_{max}, nm (ε, M^{-1} cm^{-1}): 550 (40), 705 (40). FTIR (KBr): 3541 (br), 3459 (br), 3059 (m), 2986 (w), 1759 (s, ox^{2-} C═O), 1708 (s, ox^{2-} C═O), 1670 (s, ox^{2-} C═O), 1480 (w), 1435 (w), 1393 (w), 1374 (w), 1304 (m), 1250 (w), 1192 (w), 1160 (w), 1097 (m), 1046 (w), 1008 (m), 883 (m), 836 (w), 809 (m), 790 (m), 753 (m), 710 (m), 694 (m), 578 (w), 531 (m) cm^{-1}. ^{13}C NMR (300 MHz, MeCN-d_3, δ): 166.43, 164.75, 161.00, 160.30 (all *ox*); 135.32 (d, J = 11 Hz), 133.12 (d, J = 2 Hz), 130.12 (d, J = 11 Hz) (all P*Ph*$_3$); 47.71, 9.15 (Et_3NH^+). Addition of excess Et_4NCl (2−4 equiv) to the reaction mixture affords $(Et_4N)[Re^{V}(O)(PPh_3)(ox)_2]$ by the procedure described above. Complete salt metathesis was confirmed by ^{1}H NMR spectroscopy. Samples of $[Re^{V}(O)(PPh_3)(ox)_2]^-$ for elemental analysis were obtained from concentrated EtOH solutions. The reported analysis is for $(Et_3NH)[Re^{V}(O)(PPh_3)(ox)_2]\cdot$EtOH, and the presence of one EtOH in the sample was confirmed by ^{1}H NMR spectroscopy. Anal. Calcd for $C_{30}H_{37}NO_{10}PRe$: C, 45.68; H, 4.73; N, 1.78; Found: C, 45.48; H, 4.73; N, 1.90.

Preparation of $(Et_4N)[Re^{VII}(O)_2(Br_4cat)_2]$. A 250 mL round-bottom flask was charged with a clear green solution of $(Et_4N)[Re^{V}(O)(Br_4Cat)_2(OPPh_3)]$ (1.463 g, 1.02 mmol) in acetone (75 mL) and stirred in air for 3 d, resulting in a color change to dark purple. The reaction mixture was chilled to 8 °C and purple solids precipitated from solution over 15 h. The solids were collected by vacuum filtration, washed with EtOH (2 × 15 mL, cold), and ether (2 × 15 mL), and dried in vacuo to give $(Et_4N)[Re^{VII}(O)_2(Br_4cat)_2]$ (1.097 g, 0.917 mmol, 91%) as a purple powder. UV−vis (MeCN) λ_{max}, nm (ε, M^{-1} cm^{-1}): 280 (12000), 405 (5200), 535 (5200). FAB-MS (*m*/*z*): 1066 [M-Et_4N]$^-$. FTIR (KBr): 3957 (w), 3905 (w), 2980 (w), 2362 (w), 2327 (w), 1750 (w), 1709 (w), 1538 (w), 1515 (m), 1480 (m),1454 (w), 1436 (w), 1400 (s, Br_4Cat^{2-} CC), 1358 (m), 1297 (w), 1255 (m, Br_4Cat^{2-} C−O), 1234 (m), 1172 (w), 1096 (w), 1066 (w), 999 (m), 948 (s), 922 (s), 786 (w), 756 (m), 740 (m), 692 (w), 651 (w) 576 (m) cm^{-1}. Anal. Calcd for $C_{20}H_{20}Br_8NO_6Re$: C, 20.07; H, 1.69; N, 1.17; Found: C, 20.34; H, 1.65; N, 1.32.

Preparation of $(Et_4N)[Re^{VII}(O)_2(ap^{Ph})_2]$. Method 1. Using the procedure described above for preparation of $[Re^{V}(O)(ap^{Ph})_2]^-$, $[ReO(PPh_3)_2Cl_3]$ (0.648 g, 0.780 mmol), Et_4NCl (0.512 g, 3.09 mmol), H_2ap^{Ph} (0.214 g, 0.719 mmol), MeOH (20 mL), and Et_3N (425 μL, 3.04 mmol) were combined in a sealable 100 mL flask and heated in a silicone fluid bath at 85 °C for 4 h. The resulting clear green solution containing $(Et_4N)[Re^{V}(O)(ap^{Ph})_2]$ was slowly cooled to ambient temperature and exposed to air, effecting a color change to dark violet. Slow evaporation of the solvent over 30 d deposited violet crystals, which were collected by vacuum filtration through a fritted funnel and washed with diethyl ether (2 × 15 mL) to afford $(Et_4N)[Re^{VII}(O)_2(ap^{Ph})_2]$ (0.122 g, 0.130 mmol, 18%). **Method 2.** A 20 mL scintillation vial was charged with $(Et_4N)[Re^{V}(O)(ap^{Ph})_2]$ (0.135 g, 0.146 mmol) and dissolved in 2 mL of CH_2Cl_2. Slow addition of 0.406 M pyridine *N*-oxide in CH_2Cl_2 (400 μL, 0.16 mmol) with vigorous stirring afforded an immediate color change from a pale green to a dark violet. The solution was stirred for 24 h and the solvent was removed under reduced pressure. The resulting dark powder was washed with pentane (3 × 2 mL) and dried *in vacuo* to yield $(Et_4N)[Re^{V}(O)_2(ap^{Ph})_2]$ (0.114 g, 0.121 mmol, 80%). UV−vis (CH_2Cl_2) λ_{max}, nm (ε, M^{-1} cm^{-1}): 292 (17000), 415 (sh, 6500), 494 (7500), 602 (8000). FAB-MS (*m*/*z*): 809 [M-Et_4N]$^-$. ^{1}H NMR (300 MHz, MeCN-d_3, δ): 7.34 (m, N*Ph*: ortho, meta, 8H); 7.04 (tt, J = 7, 1 Hz, N*Ph*: para, 2H); 6.43 (d, J = 2 Hz, Ar*H*, 2H); 6.08 (d, J = 2 Hz, Ar*H*, 2H); 3.42 (q, J = 7.3 Hz, $(CH_3CH_2)_4N^+$, 8H); 1.33 (tt, J = 7.3, 1.9 Hz, $(CH_3CH_2)_4N^+$, 12H) 1.25 (s, ^{t}Bu, 18H); 1.10 (s, ^{t}Bu, 18H). Anal. Calcd for $C_{48}H_{70}N_3O_4Re$: C, 61.38; H, 7.51; N, 4.47; Found: C, 61.10; H, 7.52; N, 4.44.

Reactions with Dioxygen. In a representative procedure, a 1.0 cm quartz cuvette fitted with a Kontes brand high-vacuum PTFE valve was charged with 7.5 × 10^{-5} M $[Re^{V}(O)(cat)_2]^-$ (2.0 mL, 0.0015 mmol) in CH_2Cl_2 and sealed under N_2. The solution was degassed on a high-vacuum line by three freeze−pump−thaw cycles and an initial spectrum was acquired. The cuvette was then backfilled with 1 atm of O_2 and shaken vigorously to make the initial $[O_2] \cong 9 \times 10^{-3}$ M.[89] The cuvette was placed in a Peltier UV−vis cell holder with a magnetic stirrer, and stirred to maintain a constant, large excess of dissolved O_2 throughout the reaction. The reaction progress was monitored by UV−vis spectroscopy (200−900 nm) for 35 min at 48 s intervals. For reactions with air, the solutions were similarly prepared under N_2 and degassed prior

(85) Johnson, N. P.; Lock, C. J. L.; Wilkinson, G. *J. Chem. Soc.* **1964**, 1054–66.
(86) Kettler, P. B.; Chang, Y.-D.; Zubieta, J.; Abrams, M. J. *Inorg. Chim. Acta* **1994**, *218*, 157–65.
(87) Edwards, C. F.; Griffith, W. P.; White, A. J. P.; Williams, D. J. *J. Chem. Soc., Dalton Trans.* **1992**, 957–62.
(88) Chaudhuri, P.; Verani, C. N.; Bill, E.; Bothe, E.; Weyhermueller, T.; Wieghardt, K. *J. Am. Chem. Soc.* **2001**, *123*, 2213–2223.
(89) Shirono, K.; Morimatsu, T.; Takemura, F. *J. Chem. Eng. Data* **2008**, *53*, 1867–1871.

to air exposure. For NMR kinetics studies, a J. Young brand NMR tube with a Teflon screw cap was used in place of the sealable cuvette. During the course of the reaction, the tube was shaken at ca. 5 min intervals to ensure that the concentration of dissolved O_2 was constant.

X-ray Crystallography. Crystals of $(Et_3NH)[Re^{V}(O)(ap^{Ph})_2]\cdot 0.25MeOH$, $(Et_3NH)[Re^{V}(O)(ox)_2(PPh_3)]\cdot 1.5EtOH$, and $(Et_4N)[Re^{VII}(O)_2(ap^{Ph})_2]$ suitable for X-ray diffraction analysis were coated with Paratone N oil, suspended on a small fiber loop and placed in a cooled nitrogen gas stream at 173 K on a Bruker D8 APEX II CCD sealed tube diffractometer. Data for $(Et_4N)[Re^{VII}(O)_2(ap^{Ph})_2]$ was obtained with graphite monochromated Cu Kα (λ = 1.54178 Å) radiation. Diffraction data for $(Et_3NH)[Re^{V}(O)(ap^{Ph})_2]\cdot 0.25MeOH$ and $(Et_3NH)[Re^{V}(O)(ox)_2(PPh_3)]\cdot 1.5EtOH$ were collected using graphite monochromated Mo Kα (λ = 0.71073 Å) radiation. All other data collection procedures, data processing and programs were the same for all samples. Data were measured using a series of combinations of phi and omega scans with 10 s frame exposures and 0.5° frame widths. Data collection, indexing and initial cell refinements were all carried out using APEX II software.[90] Frame integration and final cell refinements were done using SAINT software.[91] The final cell parameters were determined from least-squares refinement on 9899 reflections for $(Et_3NH)[Re^{V}(O)(ap^{Ph})_2]\cdot 0.25MeOH$, 6871 reflections for $(Et_3NH)[Re^{V}(O)(ox)_2(PPh_3)]\cdot 1.5EtOH$, and 8761 reflections for $(Et_4N)[Re^{VII}(O)_2(ap^{Ph})_2]$. The structures were solved using direct methods and difference Fourier techniques using the SHELXTL program package.[92] Hydrogen atoms were placed in their expected chemical positions using the HFIX command and were included in the final cycles of least-squares with isotropic U_{ij}'s related to the atoms ridden upon. All non-hydrogen atoms in $(Et_4N)[Re^{VII}(O)_2(ap^{Ph})_2]$ were refined anisotropically, but only the metal-containing fragments in $(Et_3NH)[Re^{V}(O)(ap^{Ph})_2]\cdot 0.25MeOH$ and $(Et_3NH)[Re^{V}(O)(ox)_2(PPh_3)]\cdot 1.5EtOH$ were refined anisotropically. Scattering factors and anomalous dispersion corrections are taken from the *International Tables for X-ray Crystallography*.[93] Other details of data collection and structure refinement are provided in Table S1.

Results

Preparation and Characterization of Oxorhenium(V) Complexes. To assay the effects of ligand redox-activity on reactions of oxorhenium(V) complexes with dioxygen, a series of structurally similar anions were prepared. Using known procedures,[73,86] $[Re^{V}(O)(cat)_2]^-$ ($[cat]^{2-}$ = 1,2-catecholate; Scheme 2) can be isolated as either a five-coordinate square pyramidal monomer or a C_1-symmetric triphenylphosphine adduct $[Re^{V}(O)(PPh_3)(cat)_2]^-$. The ^{1}H NMR spectrum of $[Re^{V}(O)(cat)_2]^-$ in MeCN-d_3 features two sharp multiplets for the equivalent $[cat]^{2-}$ ligands at 25 °C. As previously described,[86] the resonances broaden with addition of PPh_3 and separate into an eight-line pattern at −40 °C, indicative of two $[cat]^{2-}$ ligands in distinct chemical environments (Figure S1). These data indicate that the phosphine ligand in $[Re^{V}(O)(PPh_3)(cat)_2]^-$ is labile in solution at ambient temperature, but that PPh_3 binding is accompanied by *cis*−*trans* isomerization of the $[cat]^{2-}$ ligands, as observed in the solid state structures (eq 1).[86]

Further evidence of the torsional flexibility of the $[Re^{V}(O)(cat)_2]^-$ core is manifested in the structures of four homologues. Whereas $[Re^{V}(O)(PPh_3)(Br_4cat)_2]^-$ ($[Br_4cat]^{2-}$ = tetrabromo-1,2-catecholate; Scheme 2) adopts a C_1-symmetric structure with a *cis* arrangement of catecholate ligands, $[Re^{V}(O)(OPPh_3)(Br_4cat)_2]^-$ has a pseudo-C_{2v} symmetric *trans* structure in the solid state.[87] The preference for *cis* or *trans* geometry in the six-coordinate complexes can be rationalized by a consideration of the relative π-donor strength of the respective ligands; the strongest π-donor occupies the position *trans* to the oxo group,[44] and the $[X_4cat]^{2-}$ ligand has occupied π-symmetry frontier orbitals.[94] All attempts to isolate the five-coordinate $[Re^{V}(O)(Br_4cat)_2]^-$ anion were unsuccessful, presumably due to the electron-withdrawing nature of the $[Br_4cat]^{2-}$ ligand that makes the rhenium center a strong Lewis acid. However, the $OPPh_3$ ligand in $[Re^{V}(O)(OPPh_3)(Br_4cat)_2]^-$ is labile,[87] making it a suitable precursor to the $[Re^{V}(O)(Br_4cat)_2]^-$ fragment (vide infra).

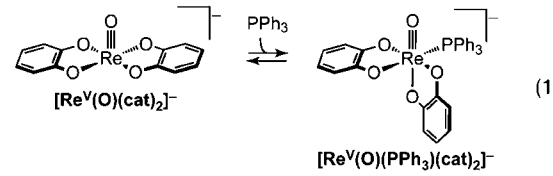

(1)

Two new oxorhenium(V) derivatives containing $[ap^{Ph}]^{2-}$ and $[ox]^{2-}$ ligands ($[ap^{Ph}]^{2-}$ = 2,4-di-*tert*-butyl-6-(phenylamido)phenolate; $[ox]^{2-}$ = ethanedioate, $C_2O_4^{2-}$) were prepared by reactions of $Re^{V}(O)(PPh_3)_2Cl_3$ with the appropriate acid ligand precursor in basic alcohol solution. Slow cooling of a concentrated solution of $(Et_3NH)[Re^{V}(O)(ap^{Ph})_2]$ deposited dark green crystals suitable for analysis by X-ray diffraction. A single crystal structure of the anion is provided in Figure 1. It contains square pyramidal rhenium bound to two crystallographically equivalent aminophenol-derived ligands in the basal positions and an oxo in the apical site. The ligand C−C bond distances are equidistant within 3σ (1.40 ± 0.01 Å), and the C−O and C−N bond distances of 1.371(4) and 1.415(5) Å, respectively, suggest that the aminophenol-derived ligands are fully reduced, closed-shell $[ap^{Ph}]^{2-}$ dianions (Table S1).[95,96] One MeOH solvent molecule is contained in each unit cell, but is not bound to rhenium. The assignment of this complex as rhenium(V) is additionally supported by the diamagnetic ^{1}H NMR spectrum and analytical data.

Crystals of $(Et_3NH)[Re^{V}(O)(PPh_3)(ox)_2]$ obtained from concentrated EtOH solution were also analyzed by X-ray diffraction. As shown in Figure 2, the anion contains rhenium with pseudo-octahedral geometry. As in the phosphine adducts described above, the PPh_3 ligand is *cis* to the oxo, so the two *cis*-oriented $[ox]^{2-}$ ligands are in distinct chemical environments. The $[ox]^{2-}$ ligand that occupies the site *trans* to PPh_3 has shorter bonds to rhenium (2.003(3) and 2.035(3) Å) and two pairs of long and short C−O bonds (averaging 1.322(5) and 1.207(5) Å, respectively) typical of a dione/diolate resonance structure (Table S1). In contrast, the $[ox]^{2-}$ *trans* to the oxo has elongated Re−O bond distances (2.092(3) and 2.082(3) Å) and a smaller difference between the average coordinated and distal C−O bond lengths (1.294(5) and 1.221(5) Å, respectively). The $Re{\equiv}O_{oxo}$ bond length of 1.671(3) Å is typical of the Re'O triple

(90) *APEX II*; Brukers AXS, Inc., Analytical X-Ray Systems: Madison, WI, 2005.
(91) *SAINT*, version 6.45A; Brukers AXS, Inc., Analytical X-ray Systems: Madison, WI, 2003.
(92) Collins, T. J. *Acc. Chem. Res.* **2002**, *35*, 782–790.
(93) *In International Tables for X-ray Crystallography, Volume C*; Wilson, J. C., Ed.; Academic Publishers: Dordrecht, The Netherlands, 1992.
(94) Bianchini, C.; Masi, D.; Mealli, C.; Meli, A.; Martini, G.; Laschi, F.; Zanello, P. *Inorg. Chem.* **1987**, *26*, 3683–93.
(95) Bill, E.; Bothe, E.; Chaudhuri, P.; Chlopek, K.; Herebian, D.; Kokatam, S.; Ray, K.; Weyhermueller, T.; Neese, F.; Wieghardt, K. *Chem.—Eur. J.* **2005**, *11*, 204–224.
(96) Poddel'sky, A. I.; Cherkasov, V. K.; Abakumov, G. A. *Coord. Chem. Rev.* **2009**, *253*, 291–324.

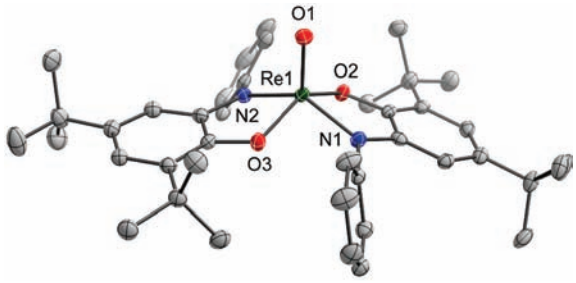

Figure 1. Solid-state structure of the anion in $(Et_3NH)[Re^{V}(O)(ap^{Ph})_2]\cdot 0.25MeOH$ shown with 50% probability ellipsoids. Hydrogen atoms, MeOH solvate molecule and countercation omitted for clarity. Selected bond lengths (Å) and angles (deg): Re1−O1 1.715(3), Re1−O2 1.968(3), Re1−O3 1.970(3), Re1−N1 1.980(3), Re1−N2 1.983(3), O1−Re1−O2 111.03(12), O1−Re1−O3 108.88(13), O1−Re1−N1 111.92(14), O1−Re1−N2 108.60(13), O2−Re1−N1 79.35(12), O3−Re1−N2 79.48(12), O2−Re1−N2 87.91(12), O3−Re1−N1 86.06(12), O2−Re1−O3 140.09(11), N1−Re1−N2 139.45(13).

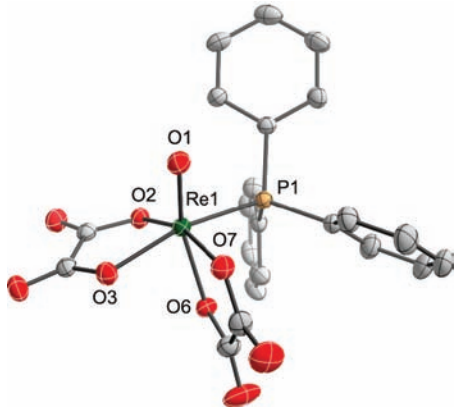

Figure 2. Solid-state structure of the anion in $(Et_3NH)[Re^{V}(O)(PPh_3)(ox)_2]\cdot 1.5EtOH$ shown with 50% probability ellipsoids. Hydrogen atoms, EtOH solvate molecule and countercation omitted for clarity. Selected bond lengths (Å) and angles (deg): Re1−O1 1.673(3), Re1−O2 2.003(3), Re1−O3 2.037(3), Re1−O6 2.092(3), Re1−O7 2.082(3), Re1−P1 2.4468(11), O1−Re1−O2 107.90(11), O1−Re1−O3 107.56(11), O1−Re1−O6 162.03(11), O1−Re1−O7 89.34(11).

bond expected for a monooxo d^2 ion in a tetragonal ligand field.[44] The diamagnetism of the $[Re^{V}(O)(PPh_3)(ox)_2]^-$ is additionally evidenced by the ^{13}C NMR spectrum, which displays four distinct resonances for the $[ox]^{2-}$ ligands in MeCN-d_3 at 25 °C, implying that isomerization is slow on the NMR time scale. However, addition of tri(4-tolyl)phosphine to NMR tubes containing $[Re^{V}(O)(PPh_3)(ox)_2]^-$ in MeCN-d_3 gives complete scrambling of the phosphine resonances within in minutes at 25 °C, indicating that the PPh_3 ligand in $[Re^{V}(O)(PPh_3)(ox)_2]^-$ is labile at ambient temperature.

Preparation and Characterization of Dioxorhenium(VII) Complexes. Addition of 1 equiv of pyridine *N*-oxide, dimethyl sulfoxide (DMSO), or $OAsPh_3$ to $[Re^{V}(O)(cat)_2]^-$ in MeCN gives an immediate color change from light tan to dark purple. The purple product is the *cis*-dioxo $[Re^{VII}(O)_2(cat)_2]^-$ anion, as evidenced by comparison of the UV−vis and ^1H NMR spectra to an authentic sample, prepared independently (eq 2).[73] When the reaction is performed in MeCN-d_3, integration of the ^1H NMR resonances confirms quantitative formation of $[Re^{VII}(O)_2(cat)_2]^-$ and the deoxygenated organic reagent: pyridine, dimethyl sulfide (DMS), or $AsPh_3$.

The analogous reaction of 1 equiv of pyridine *N*-oxide, DMSO, or $OAsPh_3$ with $[Re^{V}(O)(OPPh_3)(Br_4cat)_2]^-$, or $[Re^{V}(O)(ap^{Ph})_2]^-$ rapidly affords the corresponding dioxorhenium(VII) products. The assignment of these materials as the d^0 dioxo congeners is supported by spectroscopic and analytical data. Crystals of $(Et_4N)[Re^{VII}(O)_2(ap^{Ph})_2]$ for X-ray diffraction analysis were obtained from concentrated MeOH solution. A thermal ellipsoid plot of the anion is provided in Figure 3. The rhenium center has pseudo-octahedral geometry with approximate C_2 symmetry. Only one stereoisomer is observed in the solid-state structure. Two terminal oxo ligands occupy a pair of *cis* coordination sites, with an O−Re−O bond angle of 100.78(10)°. The remaining four sites are filled by two crystallographically unique aminophenol-derived ligands. The Re−N bonds are in an approximately *trans* disposition, with each $Re-O_{ap^{Ph}}$ bond in a site *trans* to an oxo ligand. The largest distortion from octahedral geometry is manifested in the contracted N−Re−N bond angle of 154.08(10)°. All of the C−C bond distances are identical within experimental error at 1.40 ± 0.01 Å (Table S1), consistent with a fully reduced, aromatic $[ap^{Ph}]^{2-}$ ligand.[95,96] The C−O and C−N bond lengths (averaging 1.337(6) and 1.402(6) Å, respectively) are slightly contracted versus those in $[Re^{V}(O)(ap^{Ph})_2]^-$ but within the range expected for this ligand oxidation state assignment. Further evidence for the rhenium-(VII) assignment is provided by the $Re-O_{oxo}$ bond lengths of 1.742(2) and 1.732(2) Å, which are elongated as compared to $[Re^{V}(O)(ap^{Ph})_2]^-$ due to the net decrease in formal bond order (from 3.0 to 2.5 to each oxo group) with oxygen atom addition.[44] A single crystal structure of the brominated analog $[Re^{VII}(O)_2(Br_4cat)_2]^-$ was not determined, but the structure is assigned as the *cis* conformer based on analogy to $[Re^{VII}(O)_2(cat)_2]^-$ and $[Re^{VII}(O)_2(ap^{Ph})_2]^-$.

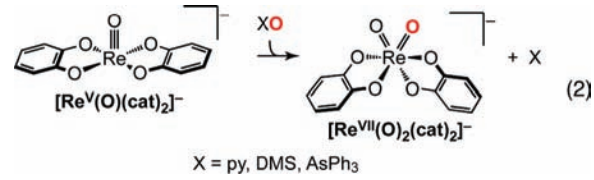

Addition of 2 equiv pyridine *N*-oxide or DMSO to violet $[Re^{V}(O)(PPh_3)(ox)_2]^-$ in MeCN rapidly gives a clear, colorless solution containing $OPPh_3$ and ReO_4^- as the only rhenium-containing product observable by ESI-MS (eq 3). [The analogous reaction of $[Re^{V}(O)(PPh_3)(ox)_2]^-$ with a stoichiometric amount of the oxidizing agent results only in conversion of the coordinated PPh_3 ligand to $OPPh_3$.] The ReO_4^- is likely a product of $[Re^{VII}(O)_2(ox)_2]^-$ decomposition; all other attempts to prepare or isolate the putative dioxo species were unsuccessful.

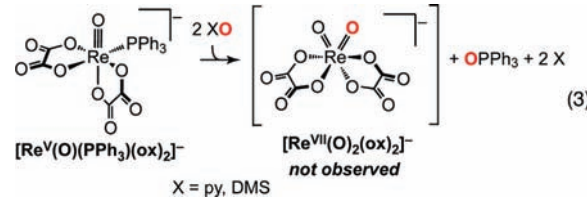

Reactions of $[Re^{V}(O)(cat)_2]^-$ with O_2. Consistent with a previous report,[73] exposure of MeCN or CH_2Cl_2 solutions of $[Re^{V}(O)(cat)_2]^-$ to 1 atm air or O_2 gives conversion to $[Re^{VII}(O)_2(cat)_2]^-$ over hours at ambient temperature. When the reaction is monitored by ^1H NMR spectroscopy in MeCN-d_3, no diamagnetic species other than $[Re^{V}(O)(cat)_2]^-$ and $[Re^{VII}(O)_2(cat)_2]^-$ accumulate to an observable concentration, and integration of the ^1H NMR resonances for $[Re^{V}(O)(cat)_2]^-$

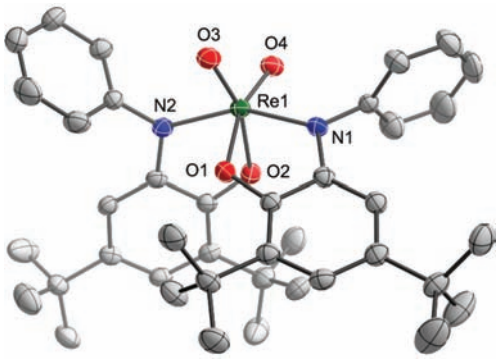

Figure 3. Solid-state structure of the anion in $(Et_4N)[Re^{VII}(O)_2(ap^{Ph})_2]$ shown with 50% probability ellipsoids. Hydrogen atoms, and countercation omitted for clarity. Selected bond lengths (Å) and angles (deg): Re1−O1 2.049(2), Re1−O2 2.040(2), Re1−O3 1.742(2), Re1−O4 1.732(2), Re1−N1 2.003(2), Re1−N2 2.036(2), O1−Re1−O2 82.23(9), O3−Re1−O4 100.78(10), O1−Re1−N1 75.55(9), O2−Re1−N2 75.23(9), O2−Re1−N1 86.38(9), O1−Re1−N2 83.87(9), O4−Re1−N2 109.73(10), O3−Re1−N1 108.14(10), O1−Re1−O4 162.25(9), O2−Re1−O3 161.95(9), N1−Re1−N2 154.08(10).

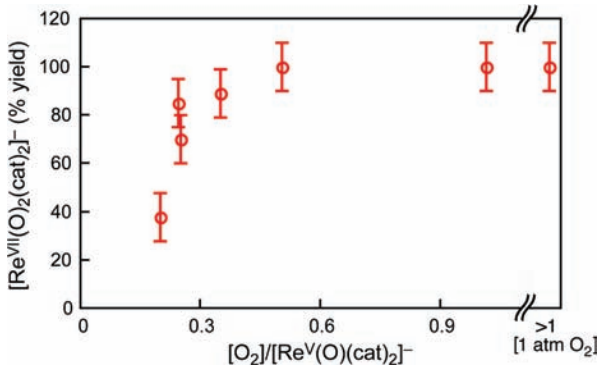

Figure 4. Plot of percent yield of $[Re^{VII}(O)_2(cat)_2]^-$ as a function of molar stoichiometry in reactions of $[Re^{V}(O)(cat)_2]^-$ with O_2 in MeCN-d_3 at 25 °C. All measurements were made in sealable NMR tubes and % conversion was determined by integration of the ^{1}H NMR resonances for $[Re^{V}(O)(cat)_2]^-$ and $[Re^{VII}(O)_2(cat)_2]^-$.

Scheme 3

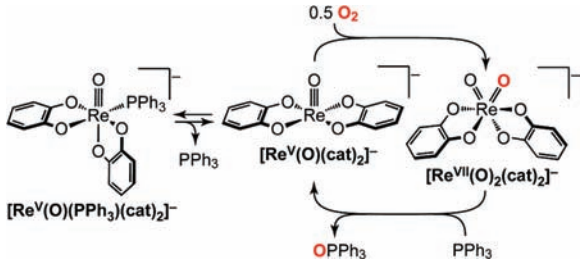

and $[Re^{VII}(O)_2(cat)_2]^-$ indicates that the total concentration of rhenium-containing products is constant throughout the reaction. Quantitative conversion of $[Re^{V}(O)(cat)_2]^-$ to $[Re^{VII}(O)_2(cat)_2]^-$ requires 0.5 equiv O_2 (Figure 4), implying that both oxygen atoms from O_2 are incorporated into Re^{VII}═O bonds.

Reaction of 1 equiv PPh_3 with $[Re^{VII}(O)_2(cat)_2]^-$ in MeCN-d_3 under N_2 gives clean conversion to $[Re^{V}(O)(cat)_2]^-$ and $OPPh_3$ in minutes, as evidenced by ^{1}H NMR spectroscopy. This closes a catalytic cycle for aerobic PPh_3 oxidation (Scheme 3). Accordingly, exposure of the triphenylphosphine adduct $[Re^{V}(O)(PPh_3)(cat)_2]^-$ to 1 atm O_2 in MeCN-d_3 affords complete conversion to $[Re^{VII}(O)_2(cat)_2]^-$ and $OPPh_3$ in 4 h at 25 °C. In contrast, NMR tubes containing $[Re^{V}(O)(PPh_3)(cat)_2]^-$ and a

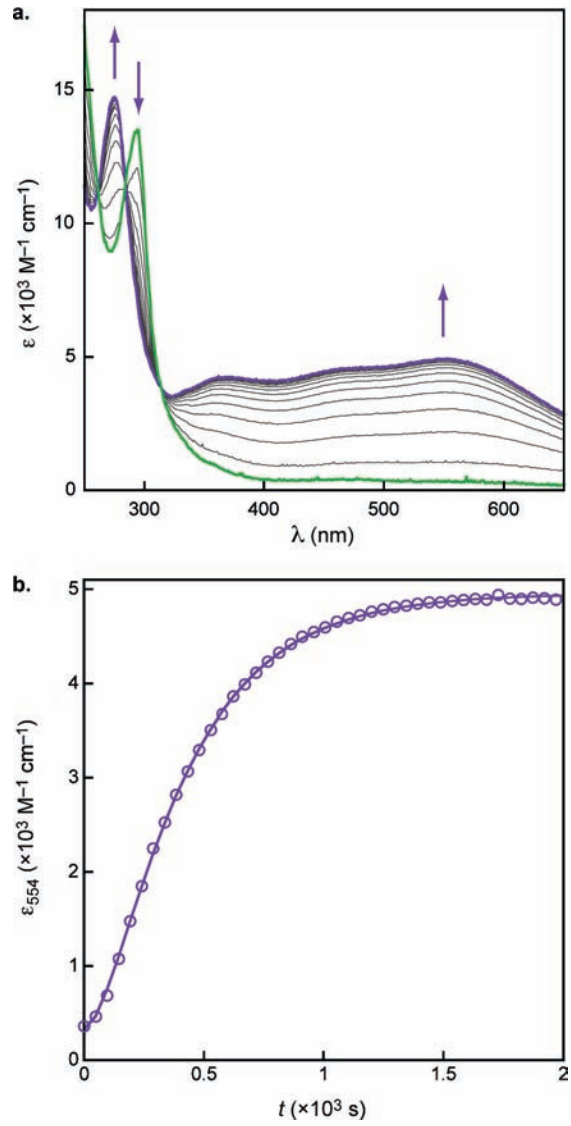

Figure 5. (a) UV−vis absorption spectra for a reaction of 8×10^{-5} M $[Re^{V}(O)(cat)_2]^-$ with 1 atm O_2 at 25 °C in CH_2Cl_2 to generate $[Re^{VII}(O)_2(cat)_2]^-$. Spectra are shown at $t = 0$ in degassed CH_2Cl_2 (green line), and at 2.4 min intervals to $t = 33.6$ min (purple line) after exposure to O_2. (b) Selected time-resolved data for the formation of $[Re^{VII}(O)_2(cat)_2]^-$ with $\lambda_{max} = 554$ nm (purple ○). The fit (purple line) was obtained from iterative analysis of the full spectral window (245−900 nm) using a biexponential A→B→C integrated rate law model, giving $k_{A\rightarrow B} = (9 \pm 1) \times 10^{-3}$ s^{-1} and $k_{B\rightarrow C} = (3 \pm 1) \times 10^{-3}$ s^{-1}.

large excess of PPh_3 (50 equiv) in MeCN-d_3 maintain their green color indefinitely in air at ambient temperature, and generation of trace $OPPh_3$ requires heating to 70 °C for 3 d. Together, these data imply that the oxidation of $[Re^{V}(O)(PPh_3)(cat)_2]^-$ by O_2 proceeds via initial preequilibrium dissociation of PPh_3 to generate $[Re^{V}(O)(cat)_2]^-$ and that a vacant site at rhenium is a prerequisite for the reaction with O_2.

The distinct color change accompanying the aerobic conversion of $[Re^{V}(O)(cat)_2]^-$ to $[Re^{VII}(O)_2(cat)_2]^-$ allows the reaction to be conveniently monitored by UV−vis absorption spectroscopy. Addition of 1 atm O_2 to 0.08 mM $[Re^{V}(O)(cat)_2]^-$ in CH_2Cl_2 affords quantitative conversion to $[Re^{VII}(O)_2(cat)_2]^-$ in 30 min with apparent isosbestic points at 260, 284, and 312 nm (Figure 5a). However, close examination of the kinetics data shows that the conversion of $[Re^{V}(O)(cat)_2]^-$ to $[Re^{VII}(O)_2(cat)_2]^-$ does not proceed in a single phase. The

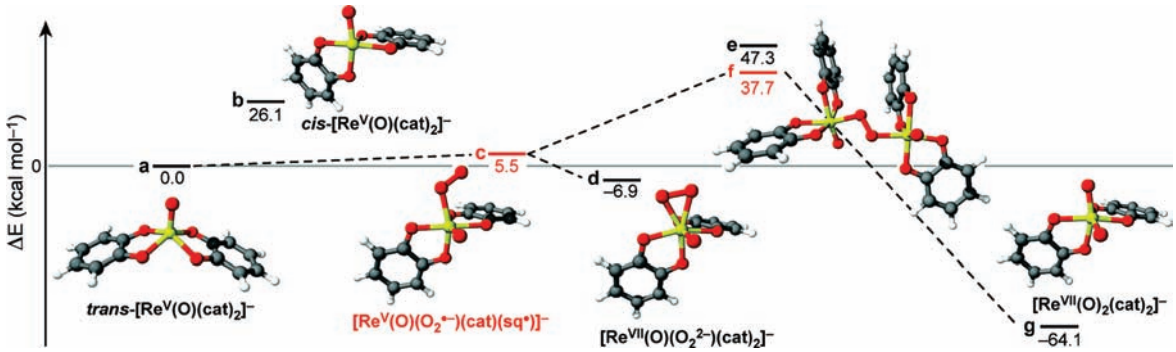

Figure 6. Reaction energy diagram for 2 $[Re^{V}(O)(cat)_2]^- + O_2 \rightarrow 2\ [Re^{VII}(O)_2(cat)_2]^-$. Bold black and red lines represent the $S = 0$ and $S = 1$ states, respectively, of the rhenium complexes shown. Reported energies are relative to (a) 2 equiv *trans*-$[Re^{V}(O)(cat)_2]^-$ + O_2.[104] (b) Optimization of $[Re^{V}(O)(cat)_2]^-$ constrained to a *cis* geometry. (c) Formation of the dioxygen adduct in the $S = 1$ state, and (d) in the $S = 0$ state. (e) Relative energy of the $S = 0$ O_2-bridged bimetallic complex. (f) Single point energy of the $S = 1$ state for the O_2-bridged complex at the $S = 0$ geometry. (g) Energy of formation of 2 equiv $[Re^{VII}(O)_2(cat)_2]^-$.

pseudofirst order kinetics plot shows a significant curvature (Figure S2), indicative of a biphasic reaction.[97] As shown in Figure 5b, the concentration−time data have a sigmoidal shape that are fit best by an A → B → C integrated rate law model with two exponential equations corresponding to consecutive first-order processes. The biphasic concentration−time profile, including the length of the apparent induction period, is reproduced exactly using different batches of $[Re^{V}(O)(cat)_2]^-$ and CH_2Cl_2 solvent, and in MeCN solutions. Additionally, the reaction with O_2 is unaffected by the radical inhibitor 2,6-di-*tert*-butyl-4-methylphenol (BHT), suggesting that the biphasic behavior is not due to trace impurities or radical chain kinetics.

The comparable rate constants for the two phases of the reaction, and the relative small spectral changes during the A→B phase, makes accurate deconvolution of the kinetics data very challenging and comparison of the rate constants problematic. However, consideration of the relative trends in rates with varying concentrations of reactants is informative. When the reaction of 0.08 mM $[Re^{V}(O)(cat)_2]^-$ is performed with dry air as the source of O_2, quantitative formation of $[Re^{VII}(O)_2(cat)_2]^-$ requires 150 min (versus 30 min with O_2). The 5-fold decrease in rate of product formation therefore scales with the relative O_2 concentration. However, at a higher initial concentration of $[Re^{V}(O)(cat)_2]^-$ (0.23 mM), both reactions are slow, and the 5-fold rate difference is lost: Generation of $[Re^{VII}(O)_2(cat)_2]^-$ from O_2 and air requires 120 and 150 min, respectively. Additionally, the sigmoidal shape of the concentration−time data is significantly less pronounced, suggesting that varying the initial concentrations of O_2 and $[Re^{V}(O)(cat)_2]^-$ impacts the rates of the A → B and B → C phases of the reaction differently. Indeed, this apparent nonlinear dependence of the rate of $[Re^{VII}(O)_2(cat)_2]^-$ formation on both O_2 concentration and $[Re^{V}(O)(cat)_2]^-$ concentration are further evidence that, despite the lack of a clearly observable intermediate, the reaction does not proceed in a single step.

Computational Studies of O_2 Homolysis by $[Re^{V}(O)(cat)_2]^-$. Attempts to isolate or further characterize intermediate species in the reaction of $[Re^{V}(O)(cat)_2]^-$ with O_2 were unsuccessful, prompting us to pursue a computational study of this process. Optimized structures and energies were computed with restricted density functional theory (DFT) with the B3LYP functional and a LACVP+* basis set.[98−100] All calculations were performed with the Jaguar program[101] except for the molecular orbital plots in Figure 7, which were computed with MOLPRO[102] and plotted in Molekel.[103] Molecular species were assumed to be in the singlet state unless otherwise noted.

In the absence of a sixth ligand, the *trans* isomer of the $[Re^{V}(O)(cat)_2]^-$ anion optimizes to a stable structure (Figure 6a) with bond distances and angles that are in excellent agreement with the solid state geometrical parameters for $[Re^{V}(O)(cat)_2]^-$.[86] Attempts to locate a stable *cis* isomer of the five-coordinate $[Re^{V}(O)(cat)_2]^-$ were unsuccessful. A constrained optimization which forced a *cis* geometry led to a structure with one imaginary vibrational frequency lying 26.1 kcal mol^{-1} above the *trans* structure (Figure 6b).[104] The interaction of $[Re^{V}(O)(cat)_2]^-$ with dioxygen was probed by placing O_2 in the vacant coordination sites of both the *cis* and *trans* five-coordinate structures and performing subsequent geometry optimization. Singlet and triplet state minima were found for dioxygen adducts to both the *cis* and *trans* isomers, but the energies of the *cis* complexes are lower than the *trans* species by 28.9 and 10.2 kcal mol^{-1} for the $S = 0$ and 1 states, respectively. These data imply that O_2 addition to $[Re^{V}(O)(cat)_2]^-$ occurs with isomerization to the *cis* conformer, analogous to PPh_3 binding (vide supra). No stable structures were found with O_2 bridges[105,106] between the rhenium center and quinoid ligands in either the *cis* or *trans* isomers of $[Re^{V}(O)(cat)_2]^-$.

The $S = 0$ and 1 states of the *cis* O_2 adducts have different geometries. Formation of the lower energy, $S = 0$ state from *trans*-$[Re^{V}(O)(cat)_2]^-$ and O_2 is favorable by 6.9 kcal mol^{-1} (Figure 6d). It has an O−O bond distance of 1.42 Å and Re−O_2 bond lengths of 1.93 and 2.02 Å. These distances are most

(97) Espenson, J. H. *Chemical Kinetics and Mechanism*, 2nd ed.; McGraw-Hill Inc.: New York, 1995.
(98) Becke, A. D. *J. Chem. Phys.* **1993**, *98*, 5648–52.
(99) Hay, P. J.; Wadt, W. R. *J. Chem. Phys.* **1985**, *82*, 299–310.
(100) Stephens, P. J.; Devlin, F. J.; Chabalowski, C. F.; Frisch, M. J. *J. Phys. Chem.* **1994**, *98*, 11623–7.
(101) *Jaguar*, version 6.5; Schrodinger, LLC: New York, 2006.
(102) MOLPRO, version 2006; Werner, H.-J.; Knowles, P. J.; Lindh, R.; Manby, F. R.; Schütz, M.; et al.; http://www.molpro.net.
(103) *MOLEKEL*, version 5.0; Flükiger, P.; Lüthi, H. P.; Portmann, S.; Weber, J.; Swiss National Supercomputing Centre CSCS: Manno, Switzerland, 2000.
(104) All of the energies displayed in Figure 6 are relative to 2 equiv *trans*-$[Re^{V}(O)(cat)_2]^-$ + O_2. In Figure 6a−d, 1 equiv *trans*-$[Re^{V}(O)(cat)_2]^-$ is a bystander in the reaction. For example, the energy at 6b is computed from the reaction: 2 *trans*-$[Re^{V}(O)(cat)_2]^-$ + O_2 → *cis*-$[Re^{V}(O)(cat)_2]^-$ + *trans*-$[Re^{V}(O)(cat)_2]^-$ + O_2. In this case, the energy of 1 *trans*-$[Re^{V}(O)(cat)_2]^-$ and 1 O_2 cancel each other out when the relative reaction energy is computed.
(105) Barbaro, P.; Bianchini, C.; Frediani, P.; Meli, A.; Vizza, F. *Inorg. Chem.* **1992**, *31*, 1523–9.
(106) Barbaro, P.; Bianchini, C.; Linn, K.; Mealli, C.; Meli, A.; Vizza, F.; Laschi, F.; Zanello, P. *Inorg. Chim. Acta* **1992**, *198−200*, 31–56.

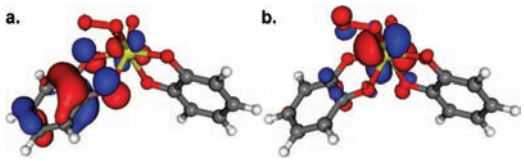

Figure 7. (a and b) Surface plots of the two orbitals with unpaired spin density in the $S = 1$ O_2-adduct to $[Re^{V}(O)(cat)_2]^-$.

consistent with formulation of dioxygen-derived ligand as an η^2-peroxo $[O_2]^{2-}$ dianion,[107,108] and the seven-coordinate complex anion as $[Re^{VII}(O)(O_2^{2-})(cat)_2]^-$. The $S = 1$ isomer is 12.4 kcal mol^{-1} higher in energy than the *cis* $S = 0$ O_2 adduct (Figure 6c). As compared to the $S = 0$ complex, the O−O bond length is contracted to 1.32 Å, and there is an enhanced asymmetry in the Re−O_2 bond distances (2.06 and 2.88 Å). Examination of the singly occupied molecular orbitals (SOMOs) for this state reveals that one unpaired electron is primarily localized in an orbital that is characteristic of a semiquinonate radical $[sq^{\bullet}]^-$ ligand (Figure 7a).[94] The other SOMO is distributed over both oxygen atoms and the metal center, with contributions from both an O−O π^* orbital and a rhenium d-orbital (Figure 7b). The large fraction of the oxygen-centered unpaired spin is on the distal atom of the O_2-derived ligand, which is antisymmetric to density on the proximal oxygen that partially overlaps with a cloverleaf metal d-orbital. The sum of these data are most consistent with formulation of the complex as rhenium(V) $[Re^{V}(O)(O_2^{\bullet-})(cat)(sq^{\bullet})]^-$ with a η^1-superoxo $[O_2^{\bullet}]^-$ ligand,[107,108] but a weak Re−O_2 π-bonding interaction transfers some radical density onto the rhenium center.

Oxygen atom transfer from $[Re^{VII}(O)(O_2^{2-})(cat)_2]^-$ to $[Re^{V}(O)(cat)_2]^-$ was probed by placing the distal oxygen of the bound O_2 ligand in the vacant coordination site of a second *cis*-$[Re^{V}(O)(cat)_2]^-$ and performing subsequent geometry optimization. All of the resulting bimetallic structures are higher in energy, consistent with Coulombic repulsion of the two anionic fragments. However, minimum energy O_2-bridged complexes were located on the potential energy surface. The $S = 0$ solution is shown in Figure 6e. The O−O distance of 1.41 Å, and the asymmetry in the Re−O_2 bond distances are most consistent with a *trans*-μ-1,2-peroxo $[O_2]^{2-}$ linkage.[107,108] No stable bimetallic structures were found with side-on, μ−η^2:η^2-peroxo linkages. A similar local minimum was not found on the $S = 1$ potential surface; however, a single point computation of the $S = 1$ energy at the optimized $S = 0$ geometry yields a lower energy (Figure 6f). This demonstrates that the triplet state potential energy surface is lower in energy than the singlet state in this region, and suggests that an $S = 1$ peroxo-bridged complex is a precursor to O_2 cleavage to generate 2 equiv $[Re^{VII}(O)_2(cat)_2]^-$.

Reactions of Oxorhenium(V) Homologues with O_2. The apparent importance of ligand-centered changes in oxidation state during O_2 homolysis by $[Re^{V}(O)(cat)_2]^-$ suggested that the reaction rates may be sensitive to substitution of the redox-active ligand. Exposure of green solutions of $[Re^{V}(O)(OPPh_3)(Br_4cat)_2]^-$ in CH_2Cl_2, MeCN or acetone to 1 atm air or O_2 results in a color change to dark purple over hours at ambient temperature. Monitoring the reaction by UV−vis absorption spectroscopy confirms that the purple product is $[Re^{VII}(O)_2(Br_4cat)_2]^-$, which is formed in quantitative yield (Figure 8a). However, in contrast to the reactions of

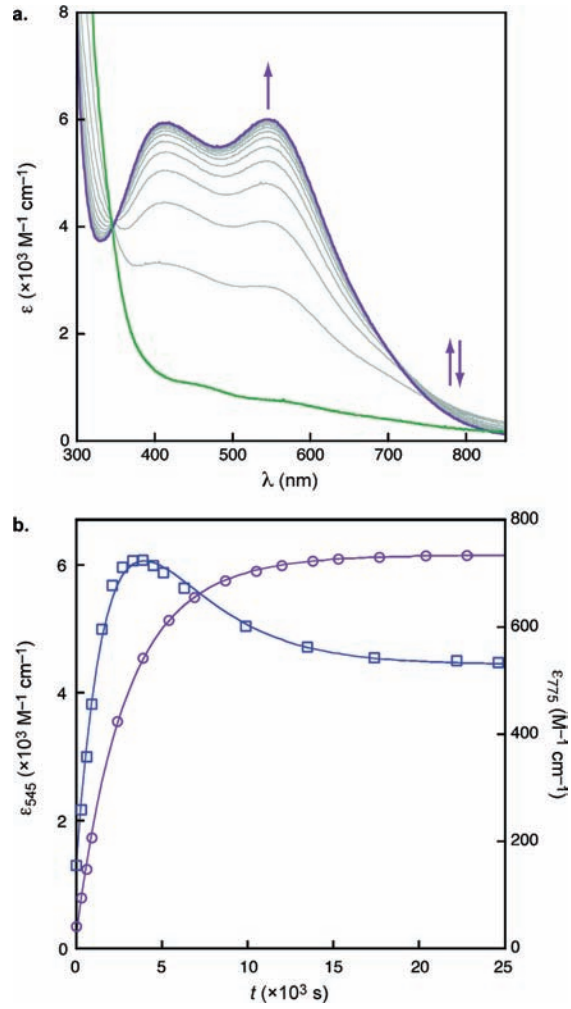

Figure 8. Selected UV−vis absorption data for a reaction of 2.0×10^{-4} M $[Re^{V}(O)(OPPh_3)(Br_4cat)_2]^-$ with 1 atm O_2 at 25 °C in CH_2Cl_2 to generate $[Re^{VII}(O)_2(Br_4cat)_2]^-$. (a) Spectra at $t = 0$, immediately on addition of O_2 (green line), and at 25.0 min intervals to $t = 500$ min (purple line). (b) Selected time-resolved data showing the formation of $[Re^{VII}(O)_2(Br_4cat)_2]^-$ with $\lambda_{max} = 545$ nm (purple ○), and the formation and decay of an intermediate species at 775 nm (blue □). The fits (purple and blue lines) were obtained simultaneously from iterative analysis of the full spectral window (300−900 nm) using a biexponential A → B → C integrated rate law model, giving $k_{A\rightarrow B} = (4.8 \pm 0.2) \times 10^{-4}$ s^{-1} and $k_{B\rightarrow C} = (2.6 \pm 0.2) \times 10^{-4}$ s^{-1}.

$[Re^{V}(O)(cat)_2]^-$ with O_2, under some conditions an intermediate species accumulates to an observable concentration during the course of the reaction. This is best evidenced by examination of the UV−vis concentration−time data from the long wavelength visible portion of the spectrum. For example, a reaction of 0.20 mM $[Re^{V}(O)(OPPh_3)(Br_4cat)_2]^-$ and 1 atm O_2 shows a growth in the absorption intensity at 775 nm over the first 3600 s of the reaction, followed by an inflection point and a decay to the $[Re^{VII}(O)_2(Br_4cat)_2]^-$ product spectrum (Figure 8b). Global iterative analysis of the full spectral window to an A → B → C integrated rate law model yields good first-order fits to both the growth and decay phases of the reaction. As described above, accurate deconvolution of the kinetics data is challenging when the computed rate constants for the two phases of the reaction are similar, making comparison of the rate constants problematic. However, under all conditions examined, the rate of formation of $[Re^{VII}(O)_2(Br_4cat)_2]^-$ from $[Re^{V}(O)(OPPh_3)(Br_4cat)_2]^-$ and O_2 is clearly slower than the parent catecholate analog. Quantitative conversion of 0.07 mM $[Re^{V}(O)(OPPh_3)(Br_4cat)_2]^-$ and 1 atm air

(107) Vaska, L. *Acc. Chem. Res.* **1976**, *9*, 175–83.
(108) Gublemann, M. H.; Williams, A. F. In *Structure and Bonding 55*; Springer-Verlag: Berlin, 1983; pp 1−65.

to $[Re^{VII}(O)_2(Br_4cat)_2]^-$ in CH_2Cl_2 requires in 1200 min (versus 150 min for the conversion of $[Re^{V}(O)(cat)_2]^-$ to $[Re^{VII}(O)_2(cat)_2]^-$ under similar conditions). All attempts to isolate the intermediate species were unsuccessful. Addition of 1 atm O_2 to a CH_2Cl_2 solution containing $[Re^{V}(O)(OPPh_3)(Br_4cat)_2]^-$ at −90 °C gives no observable color change over hours, presumably because competitive binding of $OPPh_3$ inhibits the reaction with O_2 at low temperatures. Moreover, concentrated solutions of $[Re^{V}(O)(OPPh_3)(Br_4cat)_2]^-$ in O_2 convert to $[Re^{VII}(O)_2(Br_4cat)_2]^-$ without accumulation of any observable intermediates, because the putative O_2-complex monomers are rapidly trapped by the coordinatively unsaturated $[Re^{V}(O)(Br_4cat)_2]^-$ fragment.

Exposure of lime green $[Re^{V}(O)(ap^{Ph})_2]^-$ in MeCN or CH_2Cl_2 solutions to air or O_2 immediately generates dark purple solutions containing the O_2 homolysis product $[Re^{VII}(O)_2(ap^{Ph})_2]^-$. However, the reaction yields are lower due to a competing oxidative degradation reaction that extrudes the ibq^{Ph} (ibq^{Ph} = 2,4-di-*tert*-butyl-6-(phenylimino)phenol; Scheme 2) form of the ligand. For instance, addition of 1 atm air to 0.08 mM $[Re^{V}(O)(ap^{Ph})_2]^-$ in CH_2Cl_2 affords $[Re^{VII}(O)_2(ap^{Ph})_2]^-$ in <15 min, but the yield is only about 30%. This low yield is not due to an inherent instability of the dioxo product in O_2, because independently prepared samples of $[Re^{VII}(O)_2(ap^{Ph})_2]^-$ are indefinitely stable under O_2 in solution at ambient temperature.

Notably the UV−vis spectrum of $[Re^{V}(O)(PPh_3)(ox)_2]^-$ is unchanged under 1 atm O_2 in MeCN over weeks at ambient temperature and days at 70 °C. As described above, oxidation of $[Re^{V}(O)(PPh_3)(ox)_2]^-$ by strong oxo-atom donors leads to rapid decomposition to ReO_4^-, so the comparative stability of $[Re^{V}(O)(PPh_3)(ox)_2]^-$ in O_2 implies that the $[Re^{V}(O)(ox)_2]^-$ core does not abstract an oxygen atom from O_2. Additional experimental data suggests that this inability of $[Re^{V}(O)(PPh_3)(ox)_2]^-$ to effect direct reductive cleavage of O_2 arises from kinetic and not thermodynamic factors. Heating $[Re^{V}(O)(PPh_3)(ox)_2]^-$ with 2 equiv $[Re^{VII}(O)_2(cat)_2]^-$ to 60 °C in MeCN-d_3 under N_2 affords $OPPh_3$ and 2 equiv $[Re^{V}(O)(cat)_2]^-$ in ∼5 h, as the only observable products by ^{1}H NMR spectroscopy (eq 4). The reactions presumably occur via two sequential oxygen-atom transfer reactions from $[Re^{VII}(O)_2(cat)_2]^-$, first to the labile PPh_3 and, then to $[Re^{V}(O)(ox)_2]^-$. The thermodynamics of the second step, oxo transfer from $[Re^{VII}(O)_2(cat)_2]^-$ to $[Re^{V}(O)(ox)_2]^-$ is not determined in this reaction because the equilibrium reaction may driven by the instability of $[Re^{VII}(O)_2(ox)_2]^-$. However, because $[Re^{V}(O)(cat)_2]^-$ is rapidly reoxidized under the reaction conditions, the products of eq 4 imply that $[Re^{VII}(O)_2(cat)_2]^-$ is a catalyst for the aerobic decomposition of the $[Re^{V}(O)(ox)_2]^-$ anion (Scheme 4). Indeed, heating a mixture of $[Re^{VII}(O)_2(cat)_2]^-$ and 7 equiv $[Re^{V}(O)(PPh_3)(ox)_2]^-$ under 1 atm O_2 results in complete decomposition of the oxalate complex within hours at 60 °C, conditions where $[Re^{V}(O)(PPh_3)(ox)_2]^-$ is itself stable to O_2.

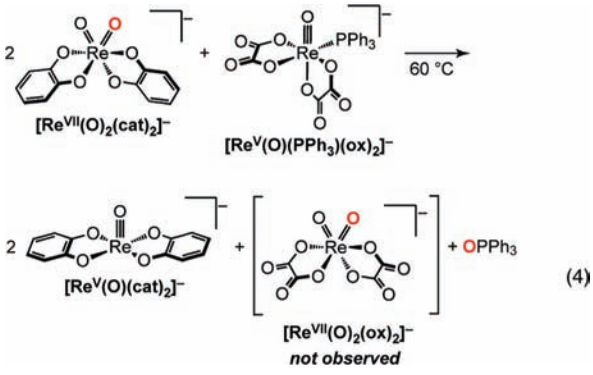

(4)

Scheme 4

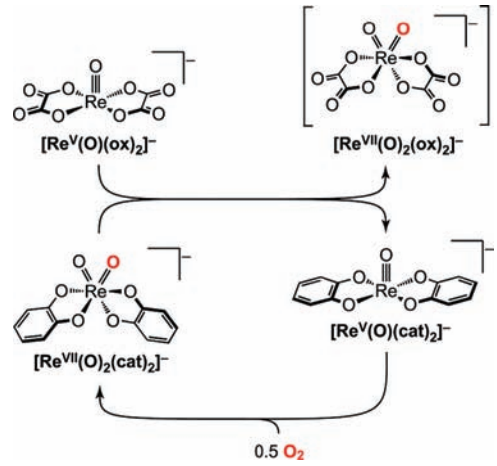

Discussion

Mechanism of O_2 Homolysis by $[Re^{V}(O)(cat)_2]^-$. The five-coordinate oxorhenium(V) anion $[Re^{V}(O)(cat)_2]^-$ effects clean reductive cleavage of dioxygen to afford the dioxorhenium(VII) product $[Re^{VII}(O)_2(cat)_2]^-$. The reaction stoichiometry (2 $[Re^{V}(O)(cat)_2]^-$ + 1 O_2 → 2 $[Re^{VII}(O)_2(cat)_2]^-$) implies that both of the dioxygen-derived atoms are consumed in formation of two new Re^{VII}=O bonds. Although a direct termolecular interaction of the three reactants is consistent with the observed stoichiometry, it is statistically and chemically implausible. Additionally, the UV−vis kinetics data for the reactions with oxygen are multiphasic and do not show a simple second order dependence on the oxorhenium(V) concentration. The sum of the experimental and computational data reported herein is most consistent with the stepwise mechanism of bimetallic O_2 homolysis shown in Scheme 5. Each of these proposed reaction steps is discussed below.

In the first step of the proposed mechanism, O_2 binding to $[Re^{V}(O)(cat)_2]^-$ generates a six-coordinate dioxygen complex. Evidence for the necessity of a vacant site at rhenium for reaction with O_2 comes from the observation that high concentrations of PPh_3 stabilize $[Re^{V}(O)(cat)_2]^-$ in O_2 atmospheres via formation of the six-coordinate species $[Re^{V}(O)(PPh_3)(cat)_2]^-$. Dioxygen-adducts to $[Re^{V}(O)(cat)_2]^-$ have not been isolated, but computational studies of these intermediates suggest that O_2 binding occurs with isomerization of the $[cat]^{2-}$ ligands to a *cis* conformation. In the absence of a sixth ligand, computations do not locate a stable *cis* isomer of $[Re^{V}(O)(cat)_2]^-$. However, a C_1-symmetry *cis* conformer may be stabilized by binding a π-acidic ligand, such as O_2, in the vacant coordination site. This ligand-driven torsional flexibility of the $[Re^{V}(O)(cat)_2]^-$ core is additionally manifest in the variable temperature ^{1}H NMR spectra of $[Re^{V}(O)(PPh_3)(cat)_2]^-$ in MeCN-d_3.[86] At −40 °C the two $[cat]^{2-}$ ligands are in distinct chemical environments, consistent with a static structure with local C_1 symmetry. However, at 25 °C the resonances for the two $[cat]^{2-}$ ligands coalesce due to PPh_3 dissociation, which affords $[Re^{V}(O)(cat)_2]^-$. The equivalent $[cat]^{2-}$ ^{1}H NMR resonances in $[Re^{V}(O)(cat)_2]^-$ are consistent with either a static C_{2v}-symmetric structure or rapid isomerization that equilibrates the ligands on the time scale of the NMR experiment. Either implicates rapid isomerization of $[Re^{V}(O)(cat)_2]^-$ with PPh_3 binding/dissociation (eq 1).

Addition of O_2 to the *cis*-$[Re^{V}(O)(cat)_2]^-$ geometry resulting from constrained optimization (Figure 6b) affords two minimum energy O_2 complexes with different spin states. As illustrated,

Scheme 5

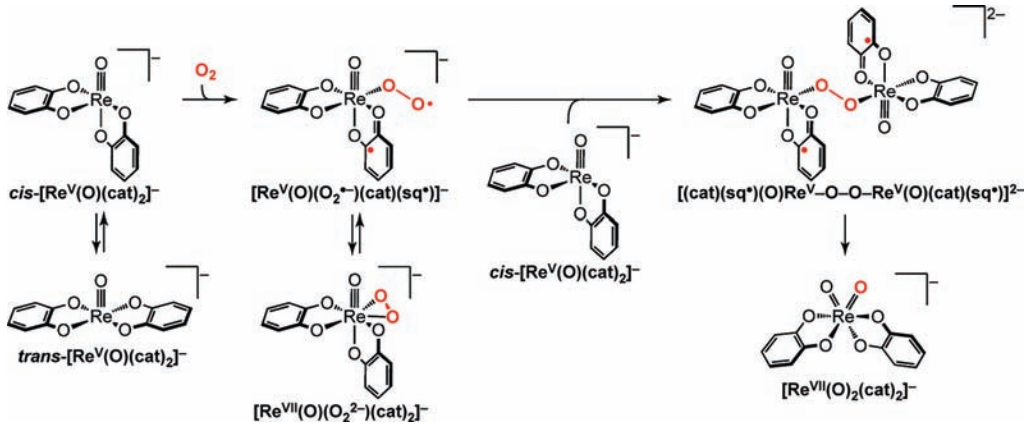

end-on approach of triplet O_2 first affords a triplet diradical complex $[Re^{V}(O)(O_2^{\bullet-})(cat)(sq^{\bullet})]^-$ containing a partially reduced η^1-superoxide $[O_2^{\bullet}]^-$ ligand. Binding and reduction of O_2 occurs with concomitant $1e^-$ oxidation of the metal fragment, but the oxidation is not metal-centered. Rather, $1e^-$ is removed from a redox-active $[cat]^{2-}$ ligand to give a semiquinonate $[sq^{\bullet}]^-$ free radical. The $S = 1$ species $[Re^{V}(O)(O_2^{\bullet-})(cat)(sq^{\bullet})]^-$ is only 5.5 kcal mol^{-1} above the ground state *trans*-$[Re^{V}(O)(cat)_2]^-$. Subsequent collapse of the distal oxygen of the η^1-superoxo ligand forms a seven-coordinate, closed-shell $S = 0$ complex containing a second Re−O_2 bond. Isomerization to the singlet state O_2-complex isomer is downhill by 12.4 kcal mol^{-1} complex, so O_2 binding to form the singlet mononuclear dioxygen complex from *trans*-$[Re^{V}(O)(cat)_2]^-$ and O_2 is exoergic by 6.9 kcal mol^{-1}. The O_2 fragment in this minimum energy complex is best described as an η^2-peroxo $[O_2]^{2-}$ dianion, implying that the $[Re^{V}(O)(cat)_2]^-$ is oxidized by $2e^-$. Both of these electrons formally derive from the rhenium center, so the complex anion is $[Re^{VII}(O)(O_2^{2-})(cat)_2]^-$, implying that spin crossover occurs with $1e^-$ reduction of the coordinated $[sq^{\bullet}]^-$ free radical. The ability of the oxorhenium(V) fragment to undergo metal-centered $2e^-$ oxidation with bond formation is well-established, as exemplified by the facile oxygen atom additions to $[Re^{V}(O)(cat)_2]^-$ described herein, as well as the rich oxo-transfer reactivity in related species.[39,48,70–72] There is also some precedent for formation of η^2-peroxo complexes of rhenium.[47,70,72,109] The importance of the redox-active $[cat]^{2-}$ ligand as a reservoir for a single electron in these reactions is discussed below.

Reaction of triplet O_2 with the closed shell $[Re^{V}(O)(cat)_2]^-$ anion is formally spin forbidden, but previous reports have suggested that such spin-forbidden reactions of O_2 with transition metals are not necessarily intrinsically slow. In particular, the reaction sequence for O_2 addition and reduction proposed here closely resembles a reaction of O_2 with a mononuclear palladium(0) species to form an η^2-peroxopalladium(II) complex.[110,111] Binding O_2 initially forms a triplet diradical palladium(I) complex with an η^1-superoxide $[O_2^{\bullet}]^-$ ligand, which crosses to a singlet surface with formation of the second Pd−O_2 bond. Delocalization of unpaired spin density onto the metal ion is proposed to lower the barrier to spin crossover to a singlet product by weakening the exchange interaction. Similarly, the formal transfer of $1e^-$ from O_2 to a redox-active catecholate ligand separates the unpaired spins in the triplet diradical complex $[Re^{V}(O)(O_2^{\bullet-})(cat)(sq^{\bullet})]^-$ (Figure 7), providing a mechanism for facile spin crossover to yield the singlet peroxorhenium(VII) product.

The second step of the proposed bimetallic homolysis mechanism is formation of a dinuclear O_2-bridged intermediate or transition state. The computed minimum-energy singlet state structure contains a *trans*-μ-1,2-peroxo $[O_2]^{2-}$ linkage. Although the net $2e^-$ reduction of O_2 could arise from either $2e^-$ oxidation of a single $[Re^{V}(O)(cat)_2]^-$ anion or from $1e^-$ oxidation of both of the terminal $[Re^{V}(O)(cat)_2]^-$ fragments, all of the computed bond distances about the two oxorhenium centers are similar, consistent with the latter, symmetric charge distribution. Accordingly, formation of the second Re−O_2 bond likely occurs with ligand-centered $1e^-$ oxidation of a second $[Re^{V}(O)(cat)_2]^-$, affording $[(cat)(sq^{\bullet})(O)Re^{V}-O-O-Re^{V}(O)(cat)(sq^{\bullet})]^{2-}$. The computed barrier to formation of the singlet peroxo-bridge complex is approximately 54 kcal mol^{-1} above singlet state monomeric peroxo complex $[Re^{VII}(O)(O_2^{2-})(cat)_2]^-$. However, calculations suggest that a triplet state potential energy surface is at least 9.6 kcal mol^{-1} lower in energy than the singlet state surface. Formation of the dinuclear peroxo-bridged intermediate is therefore proposed to proceed via initial isomerization to the excited-state triplet diradical complex $[Re^{V}(O)(O_2^{\bullet-})(cat)(sq^{\bullet})]^-$, followed by attack of the distal oxygenic radical of the η^1-superoxide $[O_2^{\bullet}]^-$ ligand on a second equivalent of $[Re^{V}(O)(cat)_2]^-$. There are strong similarities in both of the proposed Re−O_2 bond forming steps leading to assembly of a dinuclear peroxo-bridged complex: Both invoke attack of an oxygen radical on $[Re^{V}(O)(cat)_2]^-$ that proceeds with isomerization to a *cis* conformer, $1e^-$ reduction of the incoming $^{\bullet}O_2$ fragment and $1e^-$ oxidation of a redox-active $[cat]^{2-}$ ligand.

The final reaction step is homolytic cleavage of the peroxo O−O bond in $[(cat)(sq^{\bullet})(O)Re^{V}-O-O-Re^{V}(O)(cat)(sq^{\bullet})]^{2-}$ to afford 2 equiv of the dioxorhenium(VII) product $[Re^{VII}(O)_2(cat)_2]^-$. This product-forming step is formally another $2e^-$ reduction of the *trans*-μ-1,2-peroxo $[O_2]^{2-}$linkage to two terminal oxo $[O]^{2-}$ ligands. The d^0 electron count in the rhenium product suggests that intramolecular transfer of $1e^-$ from each $[Re^{V}(O)(cat)(sq^{\bullet})]$ fragment to the $[O_2]^{2-}$ group proceeds with intramolecular reduction of the coordinated semiquinonate radical $[sq^{\bullet}]^-$ ligands. As shown in Figure 6, formation of 2 equiv $[Re^{VII}(O)_2(cat)_2]^-$ from 2 equiv *trans*-$[Re^{V}(O)(cat)_2]^-$ and O_2 is favorable by 64.1 kcal mol^{-1}. Additionally, formation of 2 equiv $[Re^{VII}(O)_2(cat)_2]^-$ from 1 equiv

(109) Nicholson, T.; Zubieta, J. *Inorg. Chim. Acta* **1987**, *134*, 191–193.
(110) Landis, C. R.; Morales, C. M.; Stahl, S. S. *J. Am. Chem. Soc.* **2004**, *126*, 16302–16303.
(111) Popp, B. V.; Wendlandt, J. E.; Landis, C. R.; Stahl, S. S. *Angew. Chem., Int. Ed.* **2007**, *46*, 601–604.

trans-$[Re^{V}(O)(cat)_2]^-$ and the O_2 adduct $[Re^{VII}(O)(O_2^{2-})(cat)_2]^-$ is favorable by 57.2 kcal mol^{-1}.

The computed reaction coordinate therefore agrees well with the observed reaction kinetics: The net reaction proceeds by two sequential exoergic reaction steps, and the second step of the reaction is rate limiting. However, the observation that mononuclear O_2 adducts to $[Re^{V}(O)(cat)_2]^-$ do not accumulate to significant concentrations suggests that the computed kinetic barrier to the second step may be overestimated. Clear evidence of a biphasic reaction is obtained only in very dilute solutions, and even then, the intermediates species are fleeting. It is tempting to speculate that the intermediate observed in dilute solutions is the monomeric peroxo complex $[Re^{VII}(O)(O_2^{2-})(cat)_2]^-$, which is a minimum on the potential energy surface. This is consistent with the proposed mechanism because at high $[O_2]/[Re^{V}]$, the bulk of the $[Re^{V}(O)(cat)_2]^-$ ions are saturated with O_2, leaving them unavailable for the second step of the reaction. Yet even in dilute solutions, where the biphasic kinetics are most apparent, the second phase of the reaction is only approximately a factor of 3 slower than the first. The intermediate is consumed at a rate comparable to its formation, so reaction rates measured at higher concentrations of $[Re^{V}(O)(cat)_2]^-$ exhibit deceptively first-order concentration−time profiles that are actually composites of the two steps.

Ligand Redox Activity In 1e⁻ Reactions with Oxygenic Radicals. In total, the redox-active nature of the $[cat]^{2-}$ ligand is proposed to lower the barrier to O_2 homolysis at $[Re^{V}(O)(cat)_2]^-$ in two ways. First, both O_2 binding to $[Re^{V}(O)(cat)_2]^-$ and reaction of $[Re^{V}(O)(O_2^{\bullet-})(cat)(sq^{\bullet})]^-$ with $[Re^{V}(O)(cat)_2]^-$ formally requires 1e⁻ oxidation of $[Re^{V}(O)(cat)_2]^-$. With redox-inert ligands, this 1e⁻ necessarily derives from the rhenium(V) center, but mononuclear oxorhenium(VI) complexes are comparatively rare versus their d^0/d^2 counterparts.[48] Ligand-centered oxidation provides a pathway for 1e⁻ redox chemistry at the oxorhenium(V) ion that does not require formation of an oxorhenium(VI) species. Second, delocalization of spin density onto the redox-active ligand likely lowers the barrier to spin crossover in the formally spin-forbidden reaction of $[Re^{V}(O)(cat)_2]^-$ with O_2. This effect is similarly important in the second step of the reaction, wherein formation of the dinuclear peroxo-bridged complex likely occurs by attack of the radical superoxo group in $[Re^{V}(O)(O_2^{\bullet-})(cat)(sq^{\bullet})]^-$ on $[Re^{V}(O)(cat)_2]^-$. The triplet diradical η^1-superoxo complex is formally a spin-forbidden excited state. But the principle of microscopic reversibility predicts that the same electronic properties that facilitate spin crossover with O_2 addition also lower the barrier to isomerization to the reactive triplet species. Direct experimental evidence for the intermediacy of semiquinonate $[sq^{\bullet}]^-$ free radical species has been elusive, and the computed reaction coordinate in fact suggests that they may be short-lived. But the sum of other data provides strong, indirect support for the importance of ligand-centered redox changes in all of these elementary steps.

First, reactions with structural homologues of $[Re^{V}(O)(cat)_2]^-$ containing substituted $[cat]^{2-}$ ligands exhibit two important trends: (1) All three oxorhenium(V) complexes with redox-active catecholate and amidophenolate ligands homolyze O_2 to generate the corresponding dioxorhenium(VII) products, but $[Re^{V}(O)(ox)_2]^-$ with redox-inert oxalate ligands is inert to O_2; (2) the relative rates of O_2 homolysis parallel the oxidation potentials of the redox-active ligands, with $[ap^{Ph}]^{2-} > [cat]^{2-} > [Br_4cat]^{2-}$.[112,113] Assuming a common mechanism, the first step in the all of the reactions is O_2 binding with concomitant 1e⁻ oxidation of a redox-active ligand to form a *cis* six-coordinate complex. However the relative *cis*−*trans* isomerization rates are not likely to be a key factor in the differing rates of reaction. As described above, PPh_3 addition to $[Re^{V}(O)(Br_4cat)_2]^-$ effects facile conversion to a *cis* isomer, and the most rapid reaction with O_2 occurs at the most sterically bulky $[ap^{Ph}]^{2-}$ derivative. Additionally, these two trends cannot be rationalized by thermodynamic considerations alone (vide infra). Instead the sum of the data suggests that the ability of the redox-active ligand to provide 1e⁻ is the primary factor impacting the rates of O_2 cleavage. Moreover, the observation of ibq^{Ph} and ibq^{Ph}-derived products in reactions of with $[Re^{V}(O)(ap^{Ph})_2]^-$ with O_2 implies that ligand oxidation is viable under the reaction conditions.

Further support for the ability of redox-active ligands to mediate such 1e⁻ redox bond-forming reactions at oxorhenium(V) comes from reactions of $[Re^{V}(O)(cat)_2]^-$ with stable nitroxyl radicals, detailed in another report.[114] As shown in eq 5, addition of 2,2,6,6-tetramethylpiperidine-1-oxyl (TEMPO$^{\bullet}$) to $[Re^{V}(O)(cat)_2]^-$ gives clean conversion to $[Re^{VII}(O)_2(cat)_2]^-$ in minutes at ambient temperature. The net reaction is a very unusual oxygen-atom transfer from TEMPO$^{\bullet}$ that oxidizes the metal fragment by 2e⁻. However, the initial Re−O bond forming reaction is a spin-forbidden 1e⁻ process, wherein attack of the nitroxyl radical on *cis*-$[Re^{V}(O)(cat)_2]^-$ likely reduces TEMPO$^{\bullet}$ to the closed-shell $[TEMPO]^-$ anion (eq 6). By analogy to the chemistry described above, the $[cat]^{2-}$ ligand may supply the reducing electron required for TEMPO$^{\bullet}$ binding, generating $[sq^{\bullet}]^-$ complex intermediates. The parallels to the Re−O_2 bond-forming reactions described above are clear. In all of these reactions, the ability of the redox-active ligands to undergo 1e⁻ transfer apparently facilitates a remarkable radical-like reactivity at the closed-shell $[Re^{V}(O)(cat)_2]^-$ fragment by keying efficient Re−O bond forming reactions with oxygen radicals.

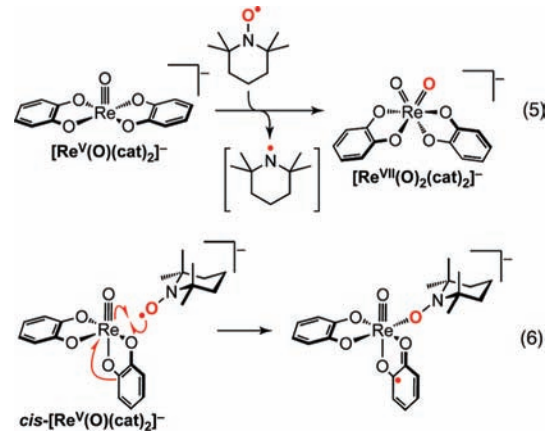

1e⁻ vs 2e⁻ Redox in O_2 Homolysis. The thermodynamic driving force for O_2 homolysis by $[Re^{V}(O)(cat)_2]^-$ and its derivatives is a function of the Re^{VII}=O bond dissociation enthalpies (BDEs) of the resulting dioxorhenium(VII) products.[39,41] All of $[Re^{V}(O)(cat)_2]^-$, $[Re^{V}(O)(Br_4cat)_2]^-$, and $[Re^{V}(O)(ap^{Ph})_2]^-$ are rapidly oxidized to the corresponding dioxo

(112) Pascaly, M.; Duda, M.; Schweppe, F.; Zurlinden, K.; Muller, F. K.; Krebs, B. *J. Chem. Soc., Dalton Trans.* **2001**, 828–837.
(113) Masui, H.; Lever, A. B. P.; Auburn, P. R. *Inorg. Chem.* **1991**, *30*, 2402–10.
(114) Lippert, C. A.; Soper, J. D. *Inorg. Chem.*, submitted for publication.

products with stoichiometric addition of 1 equiv of strong oxo donors, such as pyridine *N*-oxide, DMSO, or $OAsPh_3$. The dioxo species are all reduced by PPh_3 to regenerate the respective oxorhenium(V) anions. Together, these results bracket the Re^{VII}═O BDEs of $[Re^{VII}(O)_2(cat)_2]^-$, $[Re^{VII}(O)_2(Br_4cat)_2]^-$, and $[Re^{VII}(O)_2(ap^{Ph})_2]^-$ within the same, rather large, range 118 ± 15 kcal mol^{-1}.[115] An estimate of the Re^{VII}═O BDE in $[Re^{V}(O)(ox)_2]^-$ could not be made by this method because $[Re^{VII}(O)_2(ox)_2]^-$ is not isolable (vide supra). Accordingly, all of the bimetallic O_2 homolysis reactions are exothermic by at least 43.1 kcal mol^{-1} of rhenium, and up to 73.8 kcal mol^{-1} of rhenium, but uncertainty in determination of the respective BDEs precludes precise determination or comparison of the energetics of the individual reactions.

Given this large experimental uncertainty in the Re^{VII}═O BDEs, thermodynamic contributions to the observed differences in rates of O_2 cleavage cannot be rigorously evaluated. Because oxygen-atom addition to the oxorhenium(V) anions is formally a $2e^-$ oxidation of the metal fragment, bimetallic O_2 homolysis can be viewed as two net oxygen-atom transfers from O_2 to the metal ions. Accordingly, the spontaneity of the O_2 cleavage reaction is a function of the BDEs of the oxo acceptor substrates.[39,41] It is probable that $[Re^{V}(O)(ap^{Ph})_2]^-$, containing the most electron-rich ligand, is most easily oxidized by $2e^-$, and therefore has the most exothermic reaction with O_2. However, thermodynamics alone cannot rationalize the observed rates of reactions with O_2. In particular, the $[Re^{V}(O)(ox)_2]^-$ anion is remarkably stable in O_2. But reactions with oxidants, including DMSO, rapidly decompose $[Re^{V}(O)(ox)_2]^-$, presumably via oxo group transfer to generate $[Re^{VII}(O)_2(ox)_2]^-$. Importantly, $[Re^{V}(O)(ox)_2]^-$ also deoxygenates $[Re^{VII}(O)_2(cat)_2]^-$ (eq 4, Scheme 4). The driving force for these oxygen-atom transfer reactions may be the instability of the putative $[Re^{VII}(O)_2(ox)_2]^-$ product, but the fact that a reaction occurs at all suggests that equilibrium $2e^-$ oxo-group transfer to $[Re^{V}(O)(ox)_2]^-$ is not prohibitive. Because $[Re^{VII}(O)_2(cat)_2]^-$ is a competent catalyst for the aerobic decomposition of $[Re^{V}(O)(ox)_2]^-$, the thermodynamics of O_2 cleavage by $[Re^{V}(O)(ox)_2]^-$ are favorable (Scheme 4). The lack of a reaction with O_2 must, then, be kinetic in origin. We postulate that the source of this kinetic inhibition is the absence of an accessible $1e^-$ redox couple to mediate the $1e^-$ bond-forming steps leadings to intermediate O_2 adducts.

Implications for Bimetallic Activation and Assembly of O_2. The mechanism of O_2 homolysis by $[Re^{V}(O)(cat)_2]^-$ and its derivatives mirrors that proposed for most biological oxygenases and models systems.[19,24,25] In particular, the net $4e^-$ reduction of O_2 occurs through a series of $1e^-$ steps, via superoxo and peroxo intermediates.[25] Biological oxygenases overwhelmingly utilize naturally abundant 3d transition metal ions in their catalytic active sites, so the intermediacy of such partially reduced O_2 complexes in both natural and synthetic oxygenases is a consequence the fact that the preferred redox pathway for nearly all 3d transition metals is $1e^-$ transfer.[38] In contrast, later 4d and 5d transition metal complexes find utility in many selective bond-making and bond-breaking reactions because of their ability to mediate the transfer of multiple electrons while avoiding odd-electron intermediates. The $[Re^{V}(O)(cat)_2]^-$ ion is not structurally or electronically unique as compared to the many five-coordinate oxorhenium(V) complexes that have been extensively employed as $2e^-$ oxo-transfer reagents,[39,48,70,71] except for one factor. The catecholate ligands are redox-active, which affords access a low-energy pathway for the $1e^-$ bond-forming reactions with O_2. By way of comparison, a 2003 review[48] of oxo transfer reactions catalyzed by oxorhenium(V) complexes with redox-inert ligands highlights: (1) the scarcity of Re^{VI}, as compared to Re^{V} and Re^{VII}, and the absence of free radical reactivity; (2) the general lack of reactivity with dioxygen. The few species that do react with O_2 do not cleanly homolyze the O−O bond to generate terminal oxo ligands.[48,116] In contrast, a comparatively large number of the isoelectronic oxomolybdenum(IV) species are oxidized by O_2 to afford dioxomolybdenum(VI) complexes,[39,117] but molybdenum(V) has been noted to "intervene more directly"[48] than rhenium(VI) in oxo transfer reactions. Accordingly, for facile cleavage of O_2, an accessible $1e^-$ redox couple may be at least as important as an ability to deliver $2e^-$ in reactions with oxo-donor substrates.

The implications of this conclusion are broad. It suggests that designs for new oxygenase-type catalysts should consider not only the $2e^-$ thermodynamic stability of the resulting oxometal fragment, but also the accessibility of a $1e^-$ redox couple. Moreover, the same electronic features that facilitate bimetallic O_2 are necessarily implicit in the reverse reaction, symmetric assembly of O_2 by coupling of two metal oxo fragments. This step is commonly invoked in proposed schemes for catalytic water oxidation.[82,84] The data presented herein suggests that coupling to redox-active ligands may provide a mechanism for accessing odd-electron intermediates in the net $4e^-$ bond-forming process. To this end, one complex with redox-active quinone ligands has been shown to have good catalytic activity for water oxidation.[118,119] It is intriguing to note that computational studies suggest quinone ligand-centered redox chemistry may facilitate O−O bond formation.[118]

Conclusions

A series of five-coordinate oxorhenium(V) complexes with redox-active catecholate and amidophenolate ligands have been prepared and shown to effect clean bimetallic cleavage of O_2 to give dioxorhenium(VII) products. The rates of the O_2 homolysis reactions parallel the oxidation potentials of the redox-active ligands, with $[ap^{Ph}]^{2-} > [cat]^{2-} > [Br_4cat]^{2-}$. A structural homologue with redox-inert oxalate ligands does not react with O_2. The thermodynamics of O_2 cleavage by all of the oxorhenium(V) complexes are favorable, so thermodynamics alone can not explain the relative rates of the reactions, especially the stability of $[Re^{V}(O)(ox)_2]^-$ in O_2.

Instead, the sum of the experimental and computational data suggest that redox-active ligands lower the kinetic barrier to bimetallic O_2 homolysis at five-coordinate oxorhenium(V), by giving access to $1e^-$ redox steps that are crucial for formation and stabilization of intermediate O_2 adducts. Bimetallic O_2 activation occurs by two sequential Re−O bond forming reactions, which generate mononuclear η^1-superoxo, and then binuclear *trans*-μ-1,2-peroxo-bridged, complexes. Formation of both Re−O bonds requires trapping of a triplet radical dioxygen species by a $[Re^{V}(O)(cat)_2]^-$ anion. In each reaction the dioxygen

(115) Holm, R. H.; Kennepohl, P.; Solomon, E. I. *Chem. Rev.* **1996**, *96*, 2239–2314.
(116) Huang, R.; Espenson, J. H. *J. Mol. Catal. A: Chem.* **2001**, *168*, 39–46.
(117) Barral, R.; Bocard, C.; de Roch, I. S.; Sajus, L. *Tetrahedron Lett.* **1972**, *13*, 1693–1696.
(118) Muckerman, J. T.; Polyansky, D. E.; Wada, T.; Tanaka, K.; Fujita, E. *Inorg. Chem.* **2008**, *47*, 1787–1802.
(119) Wada, T.; Tsuge, K.; Tanaka, K. *Inorg. Chem.* **2001**, *40*, 329–337.

fragment is reduced by $1e^-$, so generation of each new Re−O bond requires that an oxometal fragment is oxidized by $1e^-$. With redox-inert ligands, this $1e^-$ necessarily derives from the rhenium(V) center. But mononuclear oxorhenium(VI) species are rare, and oxorhenium(V) complexes are not generally prone to $1e^-$ transfer or free radical reactivity. The complexes containing a redox-active ligand can access a lower energy reaction pathway for the $1e^-$ Re−O bond forming reaction because the metal fragment can be oxidized without a change in formal rhenium oxidation state. It is also likely that redox-active ligands facilitate O_2 homolysis by lowering the barrier to the formally spin-forbidden reactions of triplet dioxygen with the closed shell oxorhenium(V) anions.

Orthogonalizing $1e^-$ and $2e^-$ redox at oxorhenium(V) allows high-valent rhenium to utilize a mechanism for O_2 activation that is more typical for oxygenase enzymes and models based on 3d transition metal ions: O_2 cleavage occurs by a net $2e^-$ process through a series of $1e^-$ steps. Ongoing studies in our laboratory are pursuing the use of redox-active ligand $1e^-$ redox for multielectron oxygenase-type catalysis, as well as the microscopic reverse reaction, O−O bond formation from coupling of two M═O fragments for catalytic water oxidation.

Acknowledgment. We acknowledge the U.S. Department of Energy (Catalysis Science Grant/Contract No. DE-FG02-03ER15459 to C.D.S), the ACS Petroleum Research Fund (45130-G3 to J.D.S), a DARPA Young Faculty Award (Grant No. N6600 1-09-1-2094 to J.D.S.) and the Georgia Institute of Technology for financial support. We are grateful to Dr. Kenneth Hardcastle at Emory University for X-ray structure determination, Dr. Les Gelbaum for assistance with NMR spectroscopy, and David Bostwick for assistance with mass spectrometry.

Supporting Information Available: Variable temperature ^1H NMR for $[Re^V(O)(PPh_3)(cat)_2]^-$; tabulated X-ray metrical data; first-order plot of UV−vis kinetics data for a reaction of $[Re^V(O)(cat)_2]^-$ with O_2; Cartesian coordinates and energies for B3LYP/LACVP+* structures; X-ray crystallographic information for $(Et_3NH)[Re^V(O)(ap^{Ph})_2]\cdot 0.25MeOH$, $(Et_3NH)[Re^V(O)(PPh_3)(ox)_2]\cdot 1.5EtOH$, and $(Et_4N)[Re^{VII}(O)_2(ap^{Ph})_2]$ in CIF format. This material is available free of charge via the Internet at http://pubs.acs.org.

JA910500A